

# Spectroscopy of Faint *Kepler* Mission Exoplanet Candidate Host Stars

Mark E. Everett <sup>1</sup>, Steve B. Howell <sup>2,4</sup>, David R. Silva <sup>1</sup>, and Paula Szkody <sup>3,4</sup>

## ABSTRACT

Stellar properties are measured for a large set of *Kepler* Mission exoplanet candidate host stars. Most of these stars are fainter than 14<sup>th</sup> magnitude, in contrast to other spectroscopic follow-up studies. This sample includes many high-priority Earth-sized candidate planets. A set of model spectra are fitted to  $R \sim 3000$  optical spectra of 268 stars to improve estimates of  $T_{\text{eff}}$ ,  $\log(g)$ , and  $[\text{Fe}/\text{H}]$  for the dwarfs in the range  $4750 \leq T_{\text{eff}} \leq 7200$  K. These stellar properties are used to find new stellar radii and, in turn, new radius estimates for the candidate planets. The result of improved stellar characteristics is a more accurate representation of this *Kepler* exoplanet sample and identification of promising candidates for more detailed study. This stellar sample, particularly among stars with  $T_{\text{eff}} \gtrsim 5200$  K, includes a greater number of relatively evolved stars with larger radii than assumed by the mission on the basis of multi-color broadband photometry. About 26% of the modelled stars require radii to be revised upwards by a factor of 1.35 or greater, and modelling of 87% of the stars suggest some increase in radius. The sample presented here also exhibits a change in the incidence of planets larger than  $3 - 4R_{\oplus}$  as a function of metallicity. Once  $[\text{Fe}/\text{H}]$  increases to  $\geq -0.05$ , large planets suddenly appear in the sample while smaller planets are found orbiting stars with a wider range of metallicity. The modelled stellar spectra, as well as an additional 84 stars of mostly lower effective temperatures, are made available to the community.

*Subject headings:* planetary systems – planets and satellites: fundamental parameters – stars: fundamental parameters – surveys

## 1. INTRODUCTION

The NASA *Kepler* Mission employs a space-based 0.95 m aperture Schmidt telescope to observe a single 115 square degree field of view and obtain nearly continuous light curve coverage for over 156,000 stars. The satellite was launched in March 2009 and began science observations in May 2009 with a primary mission objective of detecting the transits of small planets orbiting near the habitable zone of Sun-like stars (Borucki et al. 2010).

---

<sup>1</sup>National Optical Astronomy Observatory, 950 N. Cherry Ave, Tucson, AZ 85719, USA

<sup>2</sup>NASA Ames Research Center, Moffett Field, CA 94035, USA

<sup>3</sup>Dept. of Astronomy, University of Washington, Seattle, WA 98195, USA

<sup>4</sup>Visiting Astronomer, Kitt Peak National Observatory, National Optical Astronomy Observatory, which is operated by the Association of Universities for Research in Astronomy (AURA) under cooperative agreement with the National Science Foundation.

Once detrended for instrumental signatures and long-term stellar variations, the *Kepler* light curves are searched for transit signals that are vetted to eliminate likely false positives (transit-like signals due to causes other than transiting planets; see Batalha et al. 2010). The periodicity and amplitude of the transits provide initial estimates for orbital periods and sizes of candidate planets. However, these planet size estimates are derived from modeling the light curves with a parameter reflecting the planet-to-star radius ratio and so depend on the uncertainty of the radius of the host star. Understanding the properties of the host stars, especially stellar radii, is therefore critical to meeting many of the mission objectives. In order to identify the most promising candidates, refine knowledge of the host star properties, and identify additional false positives, a follow-up observing program was undertaken to obtain optical spectra of candidate host stars. The resulting spectra are fitted with models to determine the three stellar properties  $T_{\text{eff}}$ ,  $\log(g)$ , and  $[\text{Fe}/\text{H}]$ . These parameters are then used to revise the stellar and candidate planet radii. This program is one of several providing ground-based follow-up reconnaissance spectroscopy of candidate exoplanet host stars as part of the *Kepler* Follow-up Program (Gautier et al. 2010).

The target sample is described in §2, the observational methods in §3, and the data reduction in §4. In §5 model fits are used to determine the stellar properties  $T_{\text{eff}}$ ,  $\log(g)$ , and  $[\text{Fe}/\text{H}]$  along with an analysis of their uncertainties. These stellar parameters are used in §6 to find fits for each star on sets of isochrones and derive revised stellar and planetary radii. The results are discussed in §7 and presented in a table listing the stellar properties for 220 candidate exoplanet host stars. The public availability of the data are discussed in §8 and the findings from these data are summarized in §9.

## 2. TARGET SAMPLE

The target stars are selected from a list of candidate exoplanet host stars known as *Kepler* Objects of Interest (KOIs) identified by the mission following a battery of tests that is designed to identify false positives. These tests include a manual inspection of each light curve and analysis of any pixel-level flux and centroid variations during the candidate transits (Batalha et al. 2010). Having passed the initial false positive identification tests unscathed, KOIs can be considered reasonable targets for planet characterization and confirmation as bona-fide planets using ground-based follow-up observations. At this point, the KOI list contains some unidentified false positives with a rate that depends on the system’s properties. Theoretical calculations have been used to predict the rate of false positives due to eclipsing binaries, especially cases where flux of a third star is blended with the eclipsing binary. Morton & Johnson (2011) predicted an overall false positive rate of 5% based on galactic structure models, the expected binary star population and eclipse depths. Later, Morton (2012) pointed out that because the KOI list still contains some candidates with V-shaped light curves, a higher false positive rate might be expected. Fressin et al. (2013) carried out a recent analysis that included simulating eclipsing binaries as background sources or as members of hierarchical triple systems and systems where true planets had their light curves blended with the flux of other stars. Their analysis predicted a higher overall false positive rate of 9.4% with a dependence on the presumed planet radius and galactic latitude. The highest false positive rate of 17.7% was predicted for giant planet candidates. Recent observational studies have also pointed toward a significant false positive rate. Santerne et al. (2012) conducted a radial velocity survey and estimated a 35% false positive rate among short-period giant planet candidates. Colón et al. (2012) used multi-color light curves to find two out of a sample of four short-period small planet KOIs were actually eclipsing binary stars, necessitating a comparably high false positive rate. Stellar classification spectroscopy can identify false positives in cases where stellar properties are found to be incorrect, however other types of observations are typically better

suited to identifying individual false positive candidates.

Our spectra were most often the first follow-up observations taken of the faint stars of interest. Up to this point, these stars have normally been characterized based only on modelling of the broadband photometry contained in the *Kepler* Input Catalog, a ground-based survey of the *Kepler* field (KIC; Brown et al. 2011). The stellar properties determined in the KIC were designed to select optimal target stars for the mission prior to launch. The ideal target stars were small (ie. dwarfs) for which transits by a given size planet produce relatively large signals. The KIC allowed *Kepler* to select mostly small stars, but within the sample, stars exhibit a range of properties that are not always accurately determined.

A list of current active KOIs is maintained by the Community Follow-up Program (CFOP<sup>5</sup>) and is continuously updated as the *Kepler* satellite observations are reduced and vetted for new candidates, or as follow-up observations help to identify some KOIs as false positives. The properties of the KOIs in our sample have likewise changed over the course of the mission. The highest priority targets, and those selected to be included in the sample, generally fall into one or more of the following categories: (1) KOIs that are requested for observation as part of an intensive study of a single star or a small number of host stars, (2) KOI stars that are candidates to be hosts of small planets ( $R_p \lesssim 2.5R_\oplus$ ), (3) KOIs in which the candidate planets orbit in a predicted habitable zone, and (4) KOI stars that harbor multiple candidate planets.

Because the KOIs are also being pursued by other spectroscopic follow-up programs and we wish to avoid unnecessary overlap, we have also selected targets on the basis of apparent brightness. The target stars span an apparent brightness range  $8 < m_{\text{Kep}} < 16$ , where  $m_{\text{Kep}}$  is the *Kepler* bandpass magnitude (Brown et al. 2011). Figure 1 shows the magnitude distribution of our target sample along with the current set of KOI stars. It also includes the magnitude distribution of those stars with new stellar radius estimates (see §6). At the bright end of the magnitude range,  $m_{\text{Kep}} < 13$ , the follow-up coverage by other groups is fairly extensive (the *Kepler* Follow-up Program reported approximately 90% of these stars as having had spectral follow-up through the 2012 observing season). To our knowledge, our spectroscopic sample is by far the largest for candidate host stars of  $m_{\text{Kep}} > 14$  ( $N = 305$ ). Such faint stars may prove too difficult or time consuming for other follow-up methods (e.g., highly precise radial velocity measurements), however they are quite important to the overall mission goals due to their large numbers (ie. two thirds of currently-active KOI stars have  $m_{\text{Kep}} > 14$  and two thirds of planet candidates with radii less than  $2.5R_\oplus$  occur around these fainter stars). A full understanding of *Kepler* exoplanet statistics requires large follow-up studies of the faint stars, or at least those of highest priority. Finally, note that a few otherwise high priority targets are excluded from the observations due to visible crowding by other stars since the modelling described here is not designed for composite spectra.

Figure 2 shows distributions of planet orbital periods and radii for the same data sets, namely our sample and that of all KOIs. The entire KOI sample is dominated by planets smaller than  $4R_\oplus$ . As *Kepler* obtains increasingly long time coverage light curves, the relative fractions of small planets and those in long-period orbits grows and the lower right hand regions in the plots of Figure 2, where habitable terrestrial planets may be located, are becoming increasingly well populated. As shown in Figure 2, the observed sample has a similar distribution to the entire KOI sample, but contains relatively fewer stars harboring large planets and relatively more candidates with long-period orbits.

---

<sup>5</sup><https://cfop.ipac.caltech.edu/>

### 3. OBSERVATIONS

We observed KOIs in the *Kepler* field (115 square degrees centered at  $\alpha = 19^{\text{h}}25^{\text{m}}$ ,  $\delta = +44.5^\circ$ ) on 48 nights during 2010 – 2012 using the National Optical Astronomy Observatory (NOAO) Mayall 4m telescope on Kitt Peak and the facility RCSpec long-slit spectrograph with one of its  $2048^2$  pixel CCDs (either T2KA or T2KB). The spectrograph configuration was the same on each observing run. The slit was  $1.0''$  wide by  $49''$  long and oriented with a position angle of  $90^\circ$ . The KPC-22b grating in second order was used to disperse the spectra with  $0.72 \text{ \AA pixel}^{-1}$  at a nominal resolution of  $\delta\lambda = 1.7\text{\AA}$ . The spectra covered a wavelength range between  $3640\text{\AA}$  and  $5120\text{\AA}$ , but were out of focus at both ends where the fluxes could not be reliably calibrated. The effective wavelength range was therefore reduced to a  $3800 - 4900\text{\AA}$  region. The scale along the slit in each spectrum was  $0.69'' \text{ pixel}^{-1}$ .

The observing procedure was basically the same each night. The telescope autoguider was used during each observation and each pointing began with an exposure of the instrument’s comparison arc lamp spectrum (HeNeAr or FeAr) for wavelength calibrations. Following that, normally a single exposure was taken of each target star. The exposure times ranged between 5 and 20 minutes for most KOIs, although a few required longer integrations due to faintness or poor observing conditions. The faintest targets requiring an exposure time exceeding 20 minutes were observed in two exposures to reduce the density of cosmic ray hits per exposure and aid in their removal during reduction. The KOIs or other stars (e.g., for flux calibrations) were all observed at an airmass of less than  $\sim 1.8$ . At the high end of this airmass range, the atmospheric dispersion for objects in the *Kepler* field remained sufficiently parallel to the slit at the latitude of Kitt Peak, and permitted efficient operations at a single instrument rotation. At least one spectrophotometric standard star selected from Massey et al. (1988) or Stone (1977) was observed each night. Calibration data consisting of bias frames, quartz lamp flat field exposures, and comparison lamp exposures were taken during the daytime.

### 4. DATA REDUCTION

The data reduction is primarily based on various IRAF<sup>6</sup> packages for performing image reduction and the *onedspec* package for extracting and calibrating the spectra. The first step is reducing the sets of bias and quartz flat lamp exposures. The overscan bias level is subtracted from each bias frame and it is trimmed to a useful data section. These bias frames are averaged to create a master. The overscan bias level is subtracted from each flat field frame followed by any (residual) bias pattern in the master bias. The flat frames are then averaged while rejecting cosmic ray hits. We normalize this master flat by fitting a smooth curve to its shape along the dispersion axis (rows) and normalizing each row of the flat by this curve. Object spectra frames are reduced by subtracting the overscan bias, trimming them, and subtracting any residual bias pattern. They are then divided by the normalized flat field.

The *onedspec* package task *doslit* is the basis of spectral extraction and calibration using the spectrophotometric standard stars. To reduce the systematic trends that may result from the variation in telescope focus with wavelength across the spectrum (a significant effect with this spectrograph configuration), a relatively wide aperture is defined to extract each spectrum. This is based on a cut through the CCD column at  $4950\text{\AA}$  where the stellar profile along the slit is broad and representative of the wavelength region used

---

<sup>6</sup>IRAF is distributed by the National Optical Astronomy Observatories, which are operated by the Association of Universities for Research in Astronomy, Inc., under cooperative agreement with the National Science Foundation.

for much of the spectral modelling. We measure sky flux in regions extracted from both sides of the stellar spectrum, and subtract it. The aperture defined by the stellar spectrum is used to extract a comparison lamp spectrum for each object. A sensitivity function is found for each night based on the ratio of the standard star to its standard curve in the IRAF database of KPNO IRS standards and used to correct the science targets and supply a relative flux level. The comparison lamp spectra are used to determine wavelength as a function of columns in order to resample the spectra to a linear wavelength scale set to closely match the sampling of the 2-D spectra.

## 5. STELLAR CHARACTERIZATION

### 5.1. Overview of the Stellar Characterization Methodology

We developed specialized software and procedures for this program. These are first used to find the basic stellar properties  $T_{\text{eff}}$ ,  $\log(g)$ , and  $[\text{Fe}/\text{H}]$ , by fitting the observed spectra to theoretical model spectra (§5). Following that, stellar and planetary radii are estimated based on the best fits of the basic stellar properties to Yale-Yonsei isochrones in (§6).

The model-fitting methods employed here rely on comparisons between observed spectra and existing synthetic spectra calculated from stellar atmosphere models and line modelling codes. Model spectra are available from the literature on a grid of discrete values for  $T_{\text{eff}}$ ,  $\log(g)$ , and  $[\text{Fe}/\text{H}]$ . The process followed here finds the best physical properties for each observed spectrum by evaluating the rms of the residuals between the observed spectrum and each model. Following that, an interpolated value is found for each stellar property by evaluating the goodness-of-fit over the grid of models. Ideally, a best-fitting model spectrum could be identified for each star and the physical properties associated with the model would then be assigned to the star. In practice, the spectral models fail to accurately predict all of the features in the observed spectra and fits often need to be restricted to specific wavelength intervals containing features that are both well represented by the models and sensitive to the parameters being sought (e.g., see Valenti & Fischer 2005). Furthermore, systematic errors in determining stellar properties can be introduced by errors in the relative spectral flux calibration and the discrete values of the model atmosphere sets. Errors in the stellar parameters can be correlated as well, complicating the situation.

In order to test the methods employed here and refine them to work on KOI stars, we observed a large number of “test stars” that have published stellar properties. Experimentation has shown that the fits can reproduce the relative stellar properties for these stars, but with systematic offsets from their literature values. The final fitting methods adopted are ones that best reproduced the literature values, once corrections for these systematic offsets were made. In essence, we adopted the test stars and their published properties as a standard set and worked to find methods that maximized the fitting precision.

The model fits are confined to a relatively narrow wavelength region at the long wavelength end of the spectra (see § 5.4). This region contains the important  $\text{H}\beta$  absorption line, which is strong in the hotter stars of our sample. Its strength and profile is dependent on effective temperature and surface gravity. Multiple atomic metal lines are also present, the strongest ones are due to low ionization states of Fe, Cr, Mn, Ni, Ti and Mg. For cooler stars, a prominent broad molecular feature appears from MgH (near 4780Å) and eventually from TiO (near 4760Å) at the lowest temperatures. These features, and the range of stellar atmosphere conditions over which they are useful diagnostics, limit the stars that we can model using these procedures. During the fitting, the strength of the metal lines drives our estimate of  $[\text{Fe}/\text{H}]$ , while the strength and profile of  $\text{H}\beta$  is largely responsible for driving the fits of  $T_{\text{eff}}$  and  $\log(g)$ . The strength of MgH

is not very well represented in the synthetic spectra (Weck et al. 2003) nor does this feature appear to be particularly helpful for fitting the cooler range of our spectra where it appears. The stars that could be fit most effectively and for which we had representative test stars were dwarfs within the effective temperature range  $4750\text{K} < T_{\text{eff}} < 7200\text{K}$  (approximate spectral types K2V through F0V) as discussed in §5.5. For this reason, only stellar properties for KOIs within this temperature range are reported here.

## 5.2. Model Spectra

The fits are based on a set of synthetic model spectra made publicly available by Coelho et al. (2005). These model spectra are calculated using their extensive line calculation codes along with the model stellar atmospheres of Castelli & Kurucz (2003). They represent predictions for non-rotating stars with relative metal abundances set to the solar values of Grevesse & Sauval (1998). The model set includes spectra calculated for stars that lie at discrete points on a 3-D grid defined by the parameters  $T_{\text{eff}}$ ,  $\log(g)$ , and  $[\text{Fe}/\text{H}]$ . The model spectra are calculated at wavelength steps of  $0.02\text{\AA}$  and with a range and spacing between adjacent values of each parameter as follows:  $T_{\text{eff}}$  between 3500 K and 7000 K in steps of 250 K,  $\log(g)$  between 1.0 and 5.0 in steps of 0.5, and  $[\text{Fe}/\text{H}]$  between  $-2.5$  and  $+0.5$  in steps of 0.5 with an additional set of models at  $[\text{Fe}/\text{H}] = +0.2$ .

## 5.3. Test Stars

The methods used to fit model spectra to the observations are the result of experiments fitting models to a set of spectra obtained for 44 test stars while attempting to reproduce the physical parameters previously published for these stars. These stars were representative of the majority of the KOIs we planned to target. Physical data taken from the literature for these stars is given in Table 1 along with the model fitting results discussed later. The test stars include a set of 20 exoplanet host stars characterized by the HATnet project (Bakos et al. 2002). The HAT stars are dwarfs ranging in  $T_{\text{eff}}$  between 4591 K and 6600 K,  $\log(g)$  between 4.13 and 4.63, and metallicities between  $-0.36$  and  $+0.41$ . Typical uncertainties in their stellar properties are 80 K for  $T_{\text{eff}}$ , 0.04 in  $\log(g)$ , and 0.08 for  $[\text{Fe}/\text{H}]$ . The atmospheric parameters of these stars have been estimated by combining spectroscopic fits with light curve modelling. The properties  $T_{\text{eff}}$  and  $[\text{Fe}/\text{H}]$  were found using the model atmospheres and line synthesis code provided by the software Spectroscopy Made Easy (SME; Valenti & Piskunov 1996) and  $\log(g)$  was found by modelling the transit light curve parameterized by the ratio of the orbital semi-major axis to the stellar radius,  $a/R_*$ , in the manner of Sozzetti et al. (2007). A second set of 6 dwarfs from the work of Valenti & Fischer (2005) was observed. These stars ranged in  $T_{\text{eff}}$  between 4969 K and 5903 K,  $\log(g)$  between 3.97 and 4.85, and  $[\text{Fe}/\text{H}]$  between  $-1.14$  and  $+0.22$  based on SME and Kurucz (1992) ATLAS9 atmosphere models. Another set of 4 dwarfs are KOIs that had also been observed by other Kepler follow-up programs using high-resolution spectroscopy (labelled with KOI or Kepler designations). These programs utilized SME along with other constraints. We also observed a number of evolved stars, including a set of 5 giants in the Kepler field for which properties have been derived from astroseismological analysis (Kallinger et al. 2010) with updated results as determined in Kallinger et al. (2012). These stars ranged in  $T_{\text{eff}}$  between 4153 K and 4893 K,  $\log(g)$  between 1.66 and 3.27, and  $[\text{Fe}/\text{H}]$  between  $-0.29$  and  $+0.18$ . A set of 8 bright giants from Luck & Heiter (2007) was included. The stellar properties adopted for this work were those Luck & Heiter (2007) derived spectroscopically using Fe I and Fe II lines. Their spectral line fits were based on MARCS (Gustafsson et al. 2003) atmosphere models and a variant of the MOOG line synthesis code (Snedden 1973). These stars had properties determined from

high-resolution spectroscopy and spanned a  $T_{\text{eff}}$  range from 4605 K to 7000 K, a  $\log(g)$  range from 2.49 to 3.31, and a  $[\text{Fe}/\text{H}]$  range from  $-0.52$  to  $+0.31$ . In addition to the giants, a single dwarf from Luck & Heiter (2007) is included.

#### 5.4. Model-Fitting Method

To determine stellar properties for both our test stars and KOI stars, we apply an iterative method of fitting model spectra to our observations, finding one stellar atmosphere parameter at a time, and in many cases holding other parameters at fixed values until the best-fitting set of stellar properties is identified. First we describe the basic procedures common to every fitting iteration, and then follow that with the details of each iteration.

To prepare the model spectra, the model data of Coelho et al. (2005) are re-binned at a wavelength sampling of  $0.3\text{\AA}$  for calculation speed. Then, for each observed spectrum, the models are resampled onto the wavelength scale of the observed spectra and smoothed using a Gaussian kernel with a FWHM of  $1.5\text{\AA}$  to match the observed resolution. Next, based on experiment, a specific wavelength interval is chosen for each fitting step. The first procedure during each iteration is to find the cross-correlation function between the observed and model spectra, where the mean fluxes of both spectra have been subtracted. We use the location of the cross-correlation function peak to shift the model spectra to match the observations (correcting for any wavelength calibration errors and, to first order, any Doppler shift). Next, with the mean flux ( $F_{\lambda}$ ) of our observed spectrum normalized (but with no normalization relative to a continuum flux done), we scale the flux of each model spectrum to minimize the rms residuals of the fit. This scaling is done with either one or two free parameters:

$$F_{\text{scaled}} = F_{\lambda}(A + B\lambda) \quad (1)$$

Here,  $F_{\lambda}$  represents the model flux, the parameter  $A$  represents a simple scaling factor, and  $B$  an additional term that corrects slope differences between the observations and model. During some iterations,  $B$  is fixed at zero. The parameter  $B$  proved to be useful in our tests and probably removes systematic errors that might otherwise adversely affect the fits.

We apply the aforementioned procedures in the following step-by-step process:

1. An initial value for  $[\text{Fe}/\text{H}]$  is found by fitting over  $\lambda = 4600 - 4890\text{\AA}$  for the full set of models while including  $B$  as a free parameter. The value of  $[\text{Fe}/\text{H}]$  for the model having the minimum rms of fitting residuals is taken as an initial estimate.
2. An initial value of  $T_{\text{eff}}$  is found by restricting our fits to models with  $[\text{Fe}/\text{H}]$  equal to that found in step 1. Here, the fit is done over the wavelength interval  $\lambda = 4810 - 4890\text{\AA}$  and  $B$  is fixed at zero. The value of  $T_{\text{eff}}$  for the model having the minimum rms of the fitting residuals is taken as an initial estimate.
3. The spectrum is refit to find  $[\text{Fe}/\text{H}]$  in the manner of step 1, but this time the model set is restricted to include only those models having  $T_{\text{eff}}$  equal to that found in step 2. See Figure 3 (top panel) for an example fit to the spectrum of KOI 2931 where  $[\text{Fe}/\text{H}]$  is determined to be 0.0 dex during an application of this step.

4. The spectrum is refit to find  $T_{\text{eff}}$  in the manner of step 2, but this time the model set is restricted to include only those models having  $[\text{Fe}/\text{H}]$  equal to that found by step 3. See Figure 3 (middle panel) for an example fit to the spectrum of KOI 2931 where  $T_{\text{eff}}$  is determined to be 5000 K during an application of this step.
5. The value of  $\log(g)$  is determined while holding fixed the values of  $[\text{Fe}/\text{H}]$  and  $T_{\text{eff}}$  at the values found in steps 3 and 4 respectively. This best-fitting model represents the best gridpoint fit to the observed spectrum. See Figure 3 (bottom panel) for an example fit to find  $\log(g) = 4.5$  for KOI 2931 during the application of this step.
6. Finally, an interpolated value for each parameter is found as described below and illustrated in Figure 4 for the case of KOI 2931. First, each parameter is fitted in turn, keeping the values for the two parameters not being fit fixed to match their values in the model found in step 5. The set of models fit is thus a function of a single parameter. The rms values of the fitting residuals for these models are considered as a function of the parameter value. To find a minimum over a continuous distribution of the parameter value, a cubic spline is fit through these data points to locate the minimum. Then a set of 3–4 points is selected surrounding this minimum and a quadratic function is fit through them. The minimum of the quadratic function is taken to be the interpolated parameter value. In cases where the minimum lies at the edge of the grid of parameter values, no interpolation can be done. The spectra in such cases are noted and their fits are treated with extra caution.

### 5.5. Calibrations Using Test Star Fits

As mentioned previously, the stellar properties derived from model fits such as those performed here are subject to systematic errors that are difficult to resolve. Instead of finding a fitting method free of such errors (which might not be possible), we have chosen to calibrate these errors based on fits to a set of test star spectra with the previously-published spectral properties described in §5.3. Once the systematic errors are properly calibrated, a post-fitting correction is possible. At the same time, this approach permits an estimate of the uncertainties in the final stellar properties.

The results of the model fits to the 44 test star spectra are given in Table 1. For each star, the previously-published properties are listed with their uncertainties. Following those are the values from the fits to our spectra (not yet corrected for the systematic errors we are attempting to quantify here). The columns under the heading “difference in values” list the value for each parameter from this work minus the previously-published value. To make the comparison, we plot the difference between our measured parameter and those from the other literature as a function of our parameter values. The results are shown in Figures 5, 6, and 7 for  $[\text{Fe}/\text{H}]$ ,  $T_{\text{eff}}$ , and  $\log(g)$  respectively. In each figure, the error bars represent the uncertainties quoted for the previously-published values. Note that in these figures, only some of the test star data are shown, namely a subset of 24 spectral fits that satisfy one or both of the following restrictions expressed in terms of the interpolated parameter values obtained during step 6 of the model fitting procedure:

$$4761\text{K} \leq T_{\text{eff}} \leq 6998\text{K} \cap \log(g) \geq 3.44 \cap [\text{Fe}/\text{H}] \geq -0.62 \quad (2)$$

$$5446\text{K} \leq T_{\text{eff}} \leq 6998\text{K} \cap \log(g) \geq 3.01 \cap [\text{Fe}/\text{H}] \geq -0.62 \quad (3)$$



The values of the parameter limits in equations 2 and 3 are chosen specifically so that after applying the corrections for systematic errors the same limits are expressed using convenient parameter values as discussed below. The reason that 20 of the 44 test star spectra are excluded from the fits is that when all of the data are plotted it became clear that only the stars falling within the restricted ranges in equations 2 and 3 behaved in a manner that would make accurate calibration possible. Furthermore, Equations 2 and 3 are chosen to exclude ranges in stellar properties that some KOIs may have, but which are not represented among our test stars. The parameters measured for stars outside of this range were either less accurate or exhibited large systematic deviations from their literature values. In any case, it is still possible to distinguish *how* the stars outside of this range differed from those inside the range (e.g., that they were cooler or had lower  $\log(g)$  values).

All three of Figures 5–7 show that there are systematic trends in the differences between the parameter values fit here and the previously-published values. Note that there are stars among this set measured using different methods, but all lie along the same linear trends. To quantify these trends, an unbiased linear least squares fit to all of the points is found and shown in the figures. These fits lead to corrective relationships that can be used to place the measured stellar properties on a scale defined by the test stars:

$$[\text{Fe}/\text{H}](\text{corr.}) = 0.4904 \times [\text{Fe}/\text{H}] + 0.0553 \quad (4)$$

$$T_{\text{eff}}(\text{corr.}) = 1.0953 \times T_{\text{eff}} - 465\text{K} \quad (5)$$

$$\log(g)(\text{corr.}) = 0.3489 \times \log(g) + 2.949 \quad (6)$$

Here, the corrected value of the parameter is labelled parenthetically with “(corr.)” and is expressed as a function of the uncorrected parameter obtained during step 6 of the method described in §5.4. Using equations 4–6, the range over which the corrections are applicable (ie. the range over which the spectral fits can be calibrated) can now be expressed in terms of the corrected stellar properties:

$$4750\text{K} \leq T_{\text{eff}} \leq 7200\text{K} \cap \log(g) \geq 4.15 \cap [\text{Fe}/\text{H}] \geq -0.25 \quad (7)$$

$$5500\text{K} \leq T_{\text{eff}} \leq 7200\text{K} \cap \log(g) \geq 4.00 \cap [\text{Fe}/\text{H}] \geq -0.25 \quad (8)$$

The scatter of points around the linear fits in Figures 5–7 provides an estimate for the uncertainties in the corrected stellar parameters. The distribution of the points around the linear fits can be described in terms of standard deviations, where  $\sigma = 0.10$  dex for  $[\text{Fe}/\text{H}]$ ,  $\sigma = 59$  K for  $T_{\text{eff}}$ , and  $\sigma = 0.13$  for  $\log(g)$ . The scatter reflects a combination of the uncertainties from the previous measurements and those presented here. To determine the contribution to the total uncertainty from the latter, one could determine an error on each parameter that, when added in quadrature to the uncertainties in the parameters quoted in the literature, would result in the linear fit having  $\chi^2_\nu = 1$ . To do this, the 1-sigma errors on the new parameter values would need to be  $\sigma([\text{Fe}/\text{H}]) = 0.066$ ,  $\sigma(T_{\text{eff}}) = 9$  K, and  $\sigma(\log(g)) = 0.12$ . Evidently for  $[\text{Fe}/\text{H}]$  and  $T_{\text{eff}}$  the uncertainties quoted for the literature values tend to dominate the total uncertainty so that this method could underestimate the uncertainty of the new parameter fits. This may be the result of at least some of the uncertainties quoted in the literature having been overestimated. In contrast, for  $\log(g)$ , the

contribution of the new uncertainties to the total error is larger and this method is useful to estimate the uncertainty.

However, since there may be unknown effects that could influence the fits, we have chosen to adopt a more conservative uncertainty on each measurement. The standard deviations of data around the fitted lines probably represents an upper limit to uncertainties within this well-characterized range of stellar properties. With that in mind, we have adopted a  $1\sigma$  uncertainty of 75 K for  $T_{\text{eff}}$ , 0.10 dex for  $[\text{Fe}/\text{H}]$ , and 0.15 for  $\log(g)$ . The stellar properties of our modelled stars are given in Table 2 and referenced by KOI number and KIC identification number.

## 6. REVISED STELLAR AND PLANETARY RADII

In total, 368 good quality spectra were obtained of 352 stars. From this master sample, 226 spectra for 220 stars had high enough quality, were not now known to harbor false positive planets, and had appropriate stellar atmospheric parameters to allow a new estimate of stellar radius and hence new estimates of exoplanet candidate radii. A total of 368 exoplanet candidates orbit these 220 stars. The Kepler magnitude distribution of these 220 stars is shown in Figure 1.

To begin, the 226 stellar spectra were separated into three  $[\text{Fe}/\text{H}]$  ranges:  $(-0.25 : -0.10)$ ,  $(-0.10 : +0.20)$ , and  $(+0.20 : +0.50)$ . Within each  $[\text{Fe}/\text{H}]$  range, measured effective temperature and surface gravity were used to estimate stellar luminosity using the so-called Version 2 Yale-Yonsei (YY) isochrones (Demarque et al. 2004) with solar abundance ratios (i.e.  $\alpha = 0$ ) and  $[\text{Fe}/\text{H}] = -0.28$ ,  $+0.04$ , and  $+0.38$ , respectively, as provided in the on-line version<sup>7</sup>. Stellar luminosity in solar units was estimated for a given  $(T_{\text{eff}}, \log(g))$  estimate by determining the median stellar luminosity in the ranges  $T_{\text{eff}} \pm 75$  K and  $\log(g) \pm 0.15$ . Given the magnitude of the  $(T_{\text{eff}}, \log(g))$  uncertainties, it was deemed appropriate to search the on-line YY Version 2 isochrone grid without further interpolation. Stellar radius in solar units was then estimated using the standard relation

$$R_{\star} = \sqrt{L_{\star}/T_{\text{eff},\star}^4} \quad (9)$$

Stellar radii uncertainties can be estimated in two ways. First, within the search box defined by the  $(T_{\text{eff}}, \log(g))$  uncertainties, the standard deviation of the mean luminosity  $\sigma_L$  can be computed. The radii uncertainty was estimated as follows:

$$\sigma_R = \left( \sqrt{(L_{\star} + \sigma_L)/T_{\text{eff},\star}^4} + \sqrt{(L_{\star} - \sigma_L)/T_{\text{eff},\star}^4} \right) / 2 \quad (10)$$

Second, 6 stars were observed at least twice and sometimes four times on separate nights during different observing runs separated by months. Stellar radius uncertainty can be estimated from the dispersion in stellar radius estimates from these individual observations. From both methods in combination, a conservative uncertainty for  $R_{\star}$  of  $\pm 0.05 R_{\odot}$  is adopted.

The new stellar radii estimates are provided in Table 2. Only a portion of this long table is presented here. The entire table is made available in the electronic version. For stars observed multiple times, individual

---

<sup>7</sup><http://www.astro.yale.edu/demarque/yyiso.html>

radii estimates were averaged into a single value. How do these new estimates compare to the best previous available radii estimates from the Kepler Science Analysis System (KSAS)<sup>8</sup>? As Figure 8 illustrates, there is a formal offset towards larger radii estimates. The radii of 87% of these stars are revised upwards (and 13% downwards), although some of these revised radii are insignificant given the uncertainties in the stellar radii. For about 26% (58) of the stars, the revised radii are skewed upwards with  $R_{\star}^{revised} \geq 1.35 \times R_{\star}^{KSAS}$ . As Figures 8 and 9 illustrate, these stars tend to be more evolved than the sample as a whole and relative to their properties listed by KSAS. In other words, it appears that many KIC stars are larger than previously assumed. In turn, exoplanet candidates orbiting those stars must be larger by the same relative amount.

Revised exoplanet candidate radii estimates can be derived from the revised stellar radii measurements from the simple geometric approximation:

$$R_p^{revised} = (R_{\star}^{revised} / R_{\star}^{KSAS}) \times R_p^{KSAS} \quad (11)$$

where initial stellar and exoplanet radii come from KSAS. Stellar radii use solar units ( $R_{\odot}$ ) while exoplanet candidate radii use Earth radius units ( $R_{\oplus}$ ). The on-line Table 3 provides the revised exoplanet candidate radii.

Figure 10 compares revised exoplanet candidate radii to the characteristics of their host stars. As previously shown by Buchhave et al. (2012) and discussed in §7, exoplanet candidates with  $R_p^{revised} \geq 4R_{\oplus}$  are much more likely to be associated with higher metallicity stars, while smaller exoplanet candidates are found around stars spanning the entire metallicity range of our sample.

## 7. DISCUSSION

The new stellar characteristics derived from this spectroscopic study have refined the properties of a large sample of KOIs, revealing statistical trends and identifying a number of individual KOIs as excellent targets for more detailed follow-up and potential confirmation as systems harboring small habitable zone planets.

In §6 we found that 26% of the KOI stars had radii significantly larger than their values based on the initial photometric data available to the mission. This effect could be due to systematic errors in the photometrically-derived stellar properties like  $\log(g)$ , selection effects in the magnitude-limited KOI sample, transit detectability dependence on stellar radius, or a combination of factors. In the case of these data, almost all of the stars with radii revised upwards by a factor of 1.35 or greater have  $T_{\text{eff}} > 5200$  K, and their positions on the  $\log(g)$ – $\log(T_{\text{eff}})$  plot of Figure 8 show that many represent a population of relatively evolved stars compared to the other stars of comparable effective temperature.

The lower  $\log(g)$  values measured here may be compared to those of Verner et al. (2011) who used asteroseismic methods on the *Kepler* light curve data to determine radii for 514 solar-type stars in the apparent magnitude range 7 – 12. For stars with  $\log(g) > 4.0$  dex and a wide range of effective temperature, the mean asteroseismic  $\log(g)$  values were 0.23 dex lower than those reported in the KIC. The corresponding stellar radii were larger as well. Another sample of stars with asteroseismic  $\log(g)$  values was compared to

---

<sup>8</sup>The KSAS was a *Kepler* Mission database storing the best available estimates for stellar and candidate planet properties. Stellar radii were based on KIC photometry for most stars in the magnitude range of interest here.

KIC  $\log(g)$  by Bruntt et al. (2012). They found asteroseismic  $\log(g)$  values were lower than those in the KIC by an average of 0.05 dex. They attributed the lower mean difference with respect to the KIC to the inclusion of stars with  $\log(g) < 4.0$  in the sample, for which asteroseismic  $\log(g)$  values are in better agreement. Verner et al. (2011) noted that their asteroseismic sample could be skewed by a Malmquist bias, which would preferentially select more evolved and intrinsically brighter stars, as well as by the improved detectability of the higher amplitude oscillations associated with stars of lower  $\log(g)$ . In the case of the spectroscopically analyzed sample presented here, the Malmquist bias would be in effect along with the counteracting bias favoring detectability of transits across smaller stars. These two biases were examined by Gaidos & Mann (2013) who predicted that the Malmquist bias would have the dominant effect, and the transit sample should be relatively overabundant in large stars compared to stars at the same temperature and apparent brightness. In addition to biases in the KOI sample as a whole, this spectroscopic sample was constructed to include many of the (relatively rare) smallest planet candidates for follow-up, a choice that may also select KOI stars with anomalous radii. It is clear that a full understanding of these biases is necessary to get better estimates for planet occurrence rates and that large, spectroscopic samples like the one presented here will play an important role. A similar spectroscopic study of “control” stars, perhaps *Kepler* stars showing no transits, may be of merit as well.

The revised values for stellar and planet radii have some implications for the mission goal to determine the frequency of Earth-sized planets orbiting Sun-like stars in a habitable zone. The radii of some planets must be revised significantly upwards, perhaps pushing them outside the size range likely for rocky Earth-like bodies. An additional effect is that higher luminosities implied by an increase in stellar radius move the habitable zones for these stars outwards from the star. As a consequence, the orbital periods of habitable zone planets must be longer.

Despite the apparent decrease in the number of small planets, these spectra provide additional evidence to favor certain candidates as among the most interesting targets for the goals of the *Kepler* Mission. An example candidate host star is KOI2931, the star shown in Figures 3 and 4. KOI2931 hosts a single known planet candidate, KOI2931.01, with an orbital period of 99.248 days. With new stellar properties  $T_{\text{eff}} = 4991$  K,  $\log(g) = 4.49$ ,  $[\text{Fe}/\text{H}] = -0.03$  and  $R_{\star} = 0.85R_{\odot}$ , the planet radius of KOI2931.01 is estimated to be  $2.1 R_{\oplus}$ . The isochrone fit for this star corresponds to a stellar mass of  $0.78M_{\odot}$  and a planet equilibrium temperature of 326 K is found assuming an albedo of 0.3 and a circular orbit. KOI2931.01 is one example of a good candidate for a super-Earth orbiting in the habitable zone.

A correlation between the incidence of relatively large planet candidates and relatively high host star metallicity (selecting large planets at  $R_p = 4.0R_{\oplus}$ ) was previously seen spectroscopically in a smaller sample of brighter KOI stars by Buchhave et al. (2012). The KOI stars in their sample were almost all brighter than  $m_{\text{kep}} = 14$ , but our and their data sets overlap in apparent brightness.

There are various ways to examine the significance of the apparent deficit of large planet candidates around low metallicity host stars ( $[\text{Fe}/\text{H}] < -0.05$ ) in this sample. First, note that 5 planet candidates in this sample (225.01, 998.01, 1067.01, 1226.01 and 1483.01) are all too large ( $> 40R_{\oplus}$ ) while the remainder are reasonable sizes for planets ( $< 20R_{\oplus}$ ). These 5 objects are considered likely false positives and excluded from further consideration. This results in 46 candidate planets orbiting host stars of  $[\text{Fe}/\text{H}] < -0.05$  and 317 orbiting host stars of  $[\text{Fe}/\text{H}] \geq -0.05$ . A K-S test comparing the planet size distributions of the these two samples reveals a difference with a confidence level of 98%. As a second test, random subsamples of 46 candidate planets are drawn from the sample of 317 candidates orbiting host stars with  $[\text{Fe}/\text{H}] \geq -0.05$  and compared to the 46 candidate planets orbiting lower metallicity stars. A set of 1 million random subsamples reveals that the most probable number of large planet candidates ( $R_p > 4R_{\oplus}$ ) orbiting high metallicity host

stars is 8 or 9, and that 2 or fewer large planet candidates occur just 0.4% of the time (2 is the number of large planet candidates orbiting the low metallicity host stars).

A fraction of the candidate planet sample may be false positives and this effect is considered next. Note that 38 known or likely false positives have already been removed from the sample of 352 stars as part of creating the candidate planet sample, but others likely remain. Also, 243 out of 363 planet candidates are members of multi-planet systems and these have a very high likelihood of being true planets rather than eclipsing binary stars (Lissauer et al. 2012). However, multi-planet systems may still be considered false positives in the sense that their planet radii can be underestimated due to host star blending (Fressin et al. 2013). A detailed treatment might be useful to simulate the effects of false positives in the sample, but a simpler approach is taken here. If a liberal reduction is made to the sample size in an effort to simulate the removal of false positives, it will weaken inferences drawn from these data. Fressin et al. (2013) predict false positive rates in five planet size ranges: 17.7% for  $R_p = 6 - 22R_\oplus$ , 15.9% for  $R_p = 4 - 6R_\oplus$ , 6.7% for  $R_p = 2 - 4R_\oplus$ , 8.8% for  $R_p = 1.25 - 2R_\oplus$  and 12.3% for  $R_p = 0.8 - 1.25R_\oplus$ . When individual planets are removed from our sample at these rates, the K-S test significance of the differences in planet size distribution on host star metallicity drops to 96%. The test of selecting random samples of high metallicity stars to match the sample size of the low metallicity stars reveals that 2 or fewer large planet candidates occur around high metallicity stars 1.7% of the time.

The tests show a dependence between host star metallicity and the occurrence rate of large transiting planets, much like for the sample of Buchhave et al. (2012). It is not surprising to see a similar pattern in these data, but the fainter stars analyzed here probe a significantly larger volume of space, showing that these effects persist across the different stellar populations. The apparent threshold value of metallicity is chosen at  $[\text{Fe}/\text{H}] = -0.05$  to match the appearance of the lower left panel in Figure 10, but the discrete and relatively sparse set of model spectra used to determine  $[\text{Fe}/\text{H}]$  may slightly distort this plot. The lines drawn at  $R_p = 4.0R_\oplus$  were also chosen by eye, but could have as well been taken at a somewhat smaller radius (ie. at  $R_p = 3 - 4R_\oplus$ ). There are no obvious trends in the incidence of planet candidates with  $R_p > 4R_\oplus$  with respect to either  $\log(g)$  or  $T_{\text{eff}}$ . Similarly, no dependence was found between metallicity and the number of planets detected around the KOI stars. Given the lack of large planets detected (in short period orbits) around low metallicity host stars, the efficiency of planet migration may be dependent on metallicity, or perhaps large planets simply cannot form around such stars at any orbital distance.

## 8. DATA AVAILABILITY

The reduced spectra and products from our model fits are made available on the CFOP website<sup>5</sup>. The CFOP website organizes data for each KOI and confirmed *Kepler* exoplanets, including the products of many follow-up observations. The data products contributed from this spectroscopy program include the reduced spectrum data files, stellar properties, plots of the spectra, fitted synthetic models plotted alongside the observed spectra (similar to Figure 3) and plots similar to Figure 4 showing the interpolation between gridpoint fit values. Additional follow-up spectra and their fits will be added in the future.

## 9. SUMMARY

A spectroscopic analysis of a large sample of stars known as *Kepler* Objects of Interest (KOIs) is presented. In the case of most of these KOIs, the stellar characterization, and by extension candidate planet

properties, had been based on broadband photometry available from the pre-launch *Kepler* Input Catalog survey. Spectral follow-up, like that presented here, proves important to improve the accuracy of the KOI stellar properties, identify interesting individual planet systems and perform accurate statistical studies of the KOI list as a whole. The results of model spectra fits (values for  $T_{\text{eff}}$ ,  $\log(g)$ , and  $[\text{Fe}/\text{H}]$ ) are given for 268 stars. Isochrone fits are used to provide revised radii for 220 KOI stars and their 368 planets. The spectra and results from this survey are made available to the public through the online CFOP archive.

The spectral and isochrone fits reveal that many of the KOI stars have larger radii than previously assumed. About 26% of the stars for which new radii were determined require corrections to their assumed radii of a factor of 1.35 or greater, and the isochrone fits for 87% of the stars suggest some increase in radius. The stars requiring the largest upward adjustment in radius represent a relatively evolved subset of the sample. The increases in stellar radii also require a reevaluation of the radii derived for the planet candidates hosted by these stars. The planet radii need to be scaled upwards by approximately the same ratio as their host stars.

Despite the fact that the revised planet radii are overall larger than previously assumed, there are candidate planets in this sample that are now better vetted and continue to be likely small planets in the habitable zone of Sun-like stars. The example of KOI2931 is presented as a good candidate for a super-Earth planet orbiting in the habitable zone of a 4991 K dwarf.

The frequency of large KOI planets in the sample depends on host star metallicity in a manner similar to that found for a sample of brighter KOI stars by Buchhave et al. (2012). The fainter, larger sample of 4750 – 7000 K dwarf KOIs analyzed in our program shows that these results extend through a larger volume of space and that the occurrence of large planets ( $R_p > 3 - 4R_{\oplus}$ ) depends on a threshold metallicity near  $[\text{Fe}/\text{H}] = -0.05$ . The large planet candidates are found almost exclusively around stars with metallicity higher than this value. In contrast, small planet candidates are found around stars spanning the full metallicity range examined in this study.

Our work was made possible through the efforts of many others. Among them are those in the *Kepler* Science Office and science team. At the telescope we always received excellent help from our observing assistants, and help from additional observers Jay Holberg, Ken Mighell, and Jason Rowe. Codes used in our modelling were adopted from work by Greg Doppmann and we received help to compile a list of properties for our test star sample from Lars Buchhave and Thomas Kallinger. We also wish to thank the referee for helpful suggestions that were incorporated into this work. Financial support for the work was provided by the NASA *Kepler* Mission and Cooperative Agreement AST-0950945 to NOAO.

Facilities: Mayall, Kepler

## REFERENCES

- Bakos, G. Á., Lázár, J., Papp, I., Sári, P. & Green, E. M. 2002, *PASP*, 114, 974
- Bakos, G. Á. et al. 2007, *ApJ*, 670, 826B
- Bakos, G. Á. et al. 2009a, *ApJ*, 696, 1950B
- Bakos, G. Á. et al. 2009b, *ApJ*, 707, 446B
- Bakos, G. Á. et al. 2011, *ApJ*, 742, 116B
- Barclay, T. et al. 2012, in prep.
- Batalha, N. M. et al. 2010, *ApJ*, 713L, 103B
- Béky, B. et al. 2011, *ApJ*, 734, 109B
- Borucki, W. J. et al. 2010, *Science*, 327, 977
- Brown, T. M., Latham, D. W., Everett, M. E., & Esquerdo, G. A. 2011, *AJ*, 142, 112
- Bruntt, H. et al. 2012, *MNRAS*, 423, 122
- Buchhave, L. A. et al. 2010, *ApJ*, 720, 1118B
- Buchhave, L. A. et al. 2011, *ApJ*, 733, 116B
- Buchhave, L. A. et al. 2012, *Nature*, 486, 375B
- Castelli, F. & Kurucz, R. L. 2003, in *Proc. of the 210th Symposium of the IAU at Uppsala University, Uppsala, Sweden, 17-21 June, 2002*. ed. by N. Piskunov, W. W. Weiss, & D. F. Gray. Published on behalf of the IAU by the Astronomical Society of the Pacific, A20
- Coelho, P., Barbuy, B., Meléndez, J., Schiavon, R. P., Castilho, B. V. 2005, *A&A*, 443, 735
- Colón, K. D., Ford, E. B. & Morehead, R. C. 2012, *MNRAS*, 426, 342
- Demarque, P., Woo, J.-H., Kim, Y.-C., Yi, S. K., 2004, *ApJS*, 155, 667D
- Doyle, L. R. 2011, *Science*, 333, 1602D
- Fischer, D. A. & Valenti, J. 2005, *ApJ*, 622, 1102
- Fressin, F. et al. 2013, *ApJ*, 766, 81
- Gaidos, E. & Mann, A. W. 2013, *ApJ*, 762, 41G
- Gautier, T. N. et al. 2010, arXiv 1001.0352
- Grevesse, N. & Sauval, A. J. 1998, *Space Sci. Rev.*, 85, 161
- Gustafsson, B., Edvardsson, B. Eriksson, K., Mizuno-Wiedner, M., Jørgensen, U. G. & Plez, B. 2003, in *ASP Conf. Proceedings Vol. 288, Stellar Atmosphere Modeling*, ed. I. Hubeny, D. Mihalas & K. Werner (San Francisco: ASP), 331
- Hartman, J. D. et al. 2009, *ApJ*, 706, 785

- Hartman, J. D. et al. 2011a, *ApJ*, 726, 52H
- Hartman, J. D. et al. 2011b, *ApJ*, 728, 138H
- Holman, M. J. et al. 2010, *Science*, 330, 51H
- Howell, S. B. et al. 2012, *ApJ*, 746, 123H
- Kallinger, T. et al. 2010, *A&A*, 522, A1
- Kallinger, T. et al. 2012, *A&A*, 541, 51K
- Kovács, G. et al. 2007, *ApJ*, 670L, 41K
- Kurucz, R. L. & Avrett, E. H. 1981, *SAOSR*, 391
- Kurucz, R. L. 1992, in *Proceedings of the 149th Symposium of the International Astronomical Union, The Stellar Populations of Galaxies*, ed. B. Barbuy & A. Renzini (Dordrecht: Kluwer), 225
- Latham, D. W. et al. 2009, *ApJ*, 704, 1107L
- Lissauer, J. L. et al. 2012, *ApJ*, 750, 112L
- Luck, R. E., & Heiter, U. 2007, *AJ*, 133, 2464
- Massey, P., Strobel, K., Barnes, J. V. & Anderson, E. 1988, *ApJ*, 328, 315
- Morton, T. D. 2012, *ApJ*, 761, 6
- Morton, T. D. & Johnson, J. A. 2011, *ApJ*, 738, 170
- Noyes, R. W. et al. 2008, *ApJ*, 673L, 79N
- Quinn, S. N. et al. 2012, *ApJ*, 745, 80Q
- Santerne, A. et al. 2012, *A&A*, 545, 76
- Snedden, C. A. 1973, PhD Thesis, Univ. of Texas, Austin
- Sozzetti, A., Torres, G., Charbonneau, D., Latham, D. W., Holman, M. J., Winn, J. N., Laird, J. B., O'Donovan, F. T. 2007, *ApJ*, 664, 1190
- Stone, R. P. S. 1977, *ApJ*, 218, 767
- Torres, G. et al. 2007, *ApJ*, 666, L121
- Torres, G. et al. 2010, *ApJ*, 715, 458T
- Valenti, J. A. & Fischer, D. A. 2005, *ApJS*, 159, 141V
- Valenti, J. A. & Piskunov, N. 1996, *A&AS*, 118, 595
- Verner, G. A. et al. 2011, *ApJ*, 738, L28
- Weck, P. F., Schweitzer, A., Stancil, P. C., Hauschildt, P. H. & Kirby, K. 2003, *ApJ*, 582, 1059



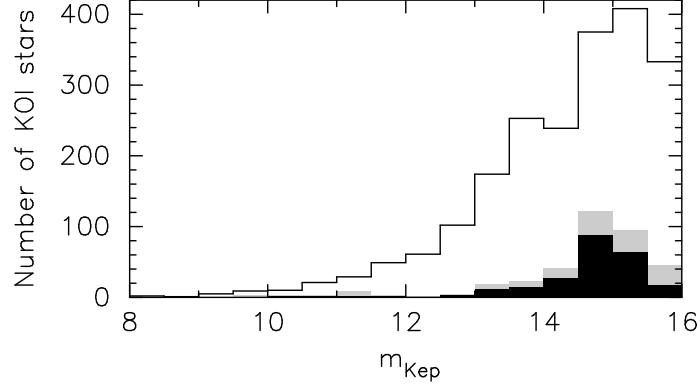


Fig. 1.— Number of KOI stars vs. Kepler magnitude. The unfilled histogram represents the entire KOI sample as of September 2012, i.e. this was the parent sample for the project described in this paper. The grey-filled histogram represents the total observed sample (see Table 2). 81% of these stars have  $m_{\text{Kep}} > 14$ . The black-filled histogram represents the sub-sample of observed stars with new radii estimates (also see Table 2).

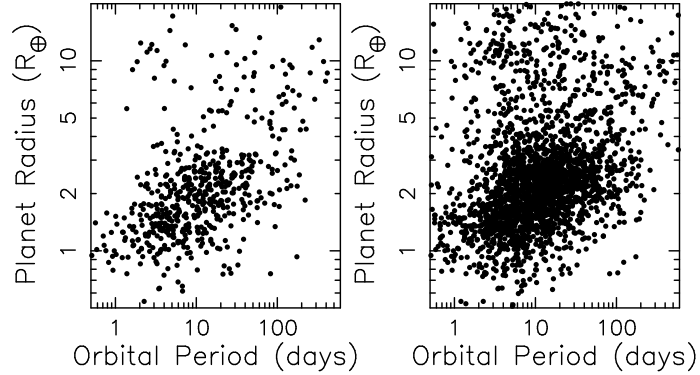


Fig. 2.— The distribution of the initial (pre-follow-up) planet radii and orbital periods for the planet candidates hosted by the observed stars (left panel) and for those around all KOI stars known as of September 2012 (right panel). Both samples are dominated by planets smaller than  $4R_{\oplus}$ , while the observed sample contains a higher fraction of small candidate planets and those in long-period orbits. See §2 for a discussion.

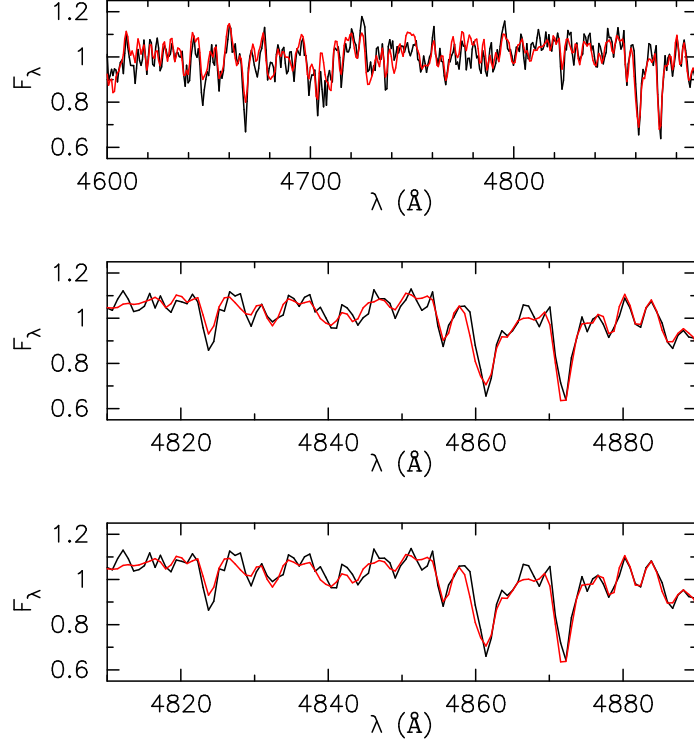


Fig. 3.— The observed spectrum of KOI 2931 in normalized flux units (in black) and model atmosphere spectrum (in red) at three steps of our model-fitting process as outlined in § 5. The top panel shows the fit to find  $[\text{Fe}/\text{H}] = 0.0$  (resulting from step 3 in our process), the middle panel shows the fit to find  $T_{\text{eff}} = 5000 \text{ K}$  (resulting from step 4 in our process), and the bottom panel shows the fit to find  $\log(g) = 4.5$  (resulting from step 5 in our process).

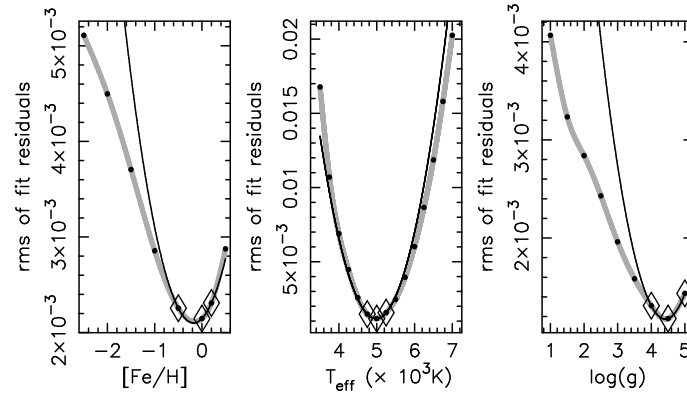


Fig. 4.— The rms of the fitting residuals (filled circles) for model spectra fits to our observations of KOI 2931 as a function of three stellar parameters and as described in § 5.4. The fits shown are for sets of models that vary in one parameter with the other two parameters fixed at their values for our best-fitting model of  $T_{\text{eff}} = 5000$  K,  $\log(g) = 4.5$ , and  $[\text{Fe}/\text{H}] = 0.0$ . The left panel shows fits as a function of  $[\text{Fe}/\text{H}]$ , the middle panel shows fits as a function of  $T_{\text{eff}}$ , and the right panel shows fits as a function of  $\log(g)$ . The grey line shows a cubic spline fit to the points. Open diamond symbols indicate three points selected to define our best parameter fit around the minimum rms value. The black lines are quadratic fits through these points whose minima represent our preliminary interpolated stellar parameters of  $T_{\text{eff}} = 4985$  K,  $\log(g) = 4.42$ , and  $[\text{Fe}/\text{H}] = +0.17$ . These values are later corrected for systematic trends as discussed in § 5.5.

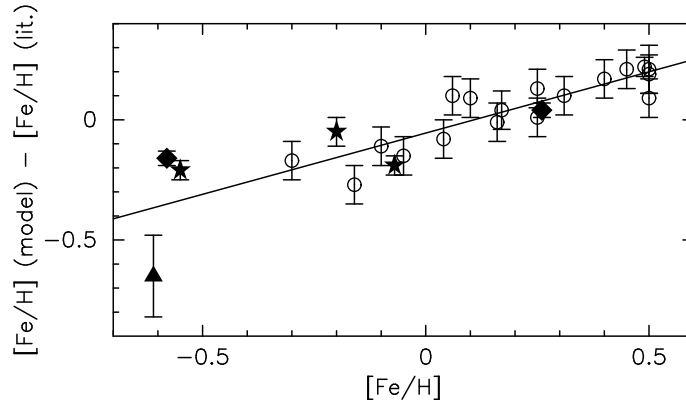


Fig. 5.— A comparison of preliminary interpolated  $[\text{Fe}/\text{H}]$  values found for 24 test stars of main sequence luminosity class to the values previously reported in the literature. The abscissa values are the preliminary interpolated  $[\text{Fe}/\text{H}]$  while the ordinate shows the difference between these values and those from the literature. Error bars represent the uncertainties quoted for the  $[\text{Fe}/\text{H}]$  values in the literature. The straight line shows an unbiased least-squares fit through the points and defines a correction to be made to remove systematic errors in the preliminary  $[\text{Fe}/\text{H}]$  estimates. This correction results in the final adopted  $[\text{Fe}/\text{H}]$  estimates. The scatter around the fit provides an estimate for the  $[\text{Fe}/\text{H}]$  uncertainties. On this plot, open circles represent HAT Project exoplanet host stars, the filled triangle is the relatively hot dwarf from Luck & Heiter (2007), star-shaped symbols are various KOI stars, and the diamonds represent stars from Valenti & Fischer (2005).

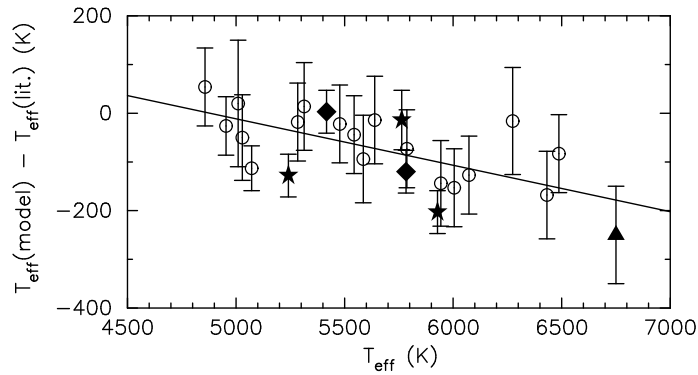


Fig. 6.— A comparison of preliminary interpolated  $T_{\text{eff}}$  values found for 24 test stars of main sequence luminosity class to the values previously reported in the literature. The abscissa values are the preliminary interpolated  $T_{\text{eff}}$  while the ordinate shows the difference between these values and those from the literature. Error bars represent the uncertainties quoted for the  $T_{\text{eff}}$  values in the literature. The straight line shows an unbiased least-squares fit through the points and defines a correction to be made to remove systematic errors in the preliminary  $T_{\text{eff}}$  estimates. This correction results in the final adopted  $T_{\text{eff}}$  estimates. The scatter around the fit provides an estimate for the  $T_{\text{eff}}$  uncertainties. See Figure 5 for an explanation of the plotting symbols.

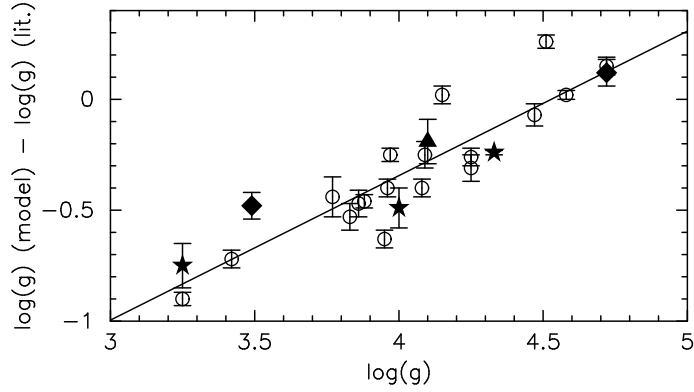


Fig. 7.— A comparison of preliminary interpolated  $\log(g)$  values found for 24 test stars of main sequence luminosity class to the values previously reported in the literature. The abscissa values are the preliminary interpolated  $\log(g)$  while the ordinate shows the difference between these values and those from the literature. Error bars represent the uncertainties quoted for the  $\log(g)$  values in the literature. The straight line shows an unbiased least-squares fit through the points and defines a correction to be made to remove systematic errors in the preliminary  $\log(g)$  estimates. This correction results in the final adopted  $\log(g)$  estimates. The scatter around the fit provides an estimate for the  $\log(g)$  uncertainties. See Figure 5 for an explanation of the plotting symbols.

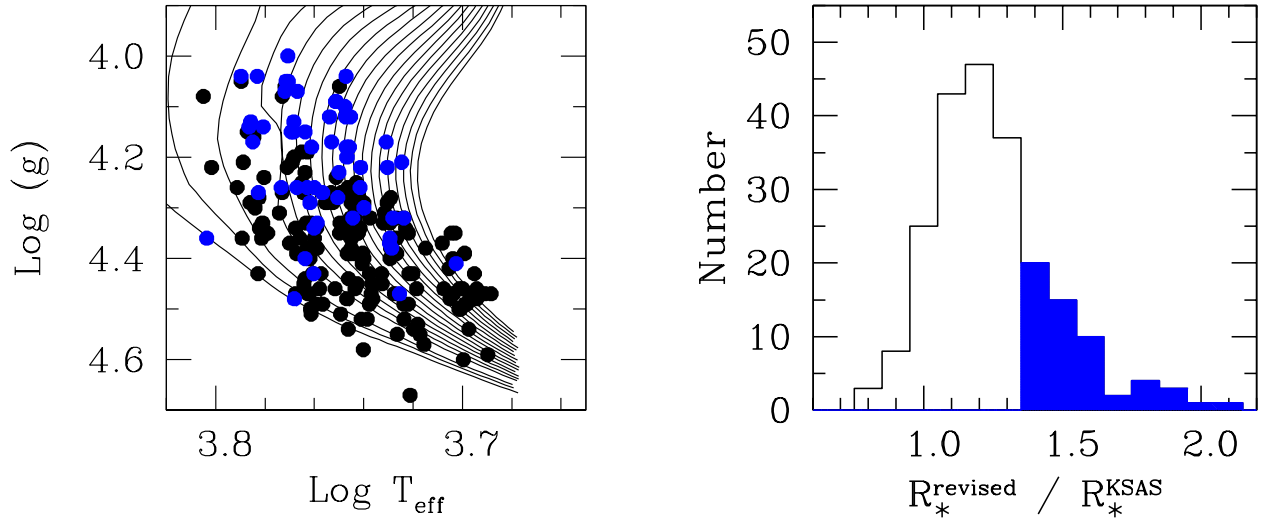


Fig. 8.— *Left panel:* The 220 stars (large black and blue circles) with new radii measurements compared to solar metallicity Version 2 Yale-Yonsei isochrones. Metal-poor and metal-rich isochrones were used to estimate stellar radii but are not shown here. Stars with blue points have revised radii  $\geq 1.35$  times their KSAS radii. *Right panel:* Distribution of  $R_*^{\text{revised}} / R_*^{\text{KSAS}}$ , where stars with revised radii  $\geq 1.35$  times their KSAS radii are indicated by solid blue bins. Clearly, stars with larger revised radii tend to be more evolved than previously assumed. (The data used to create this figure are available in the online journal.)

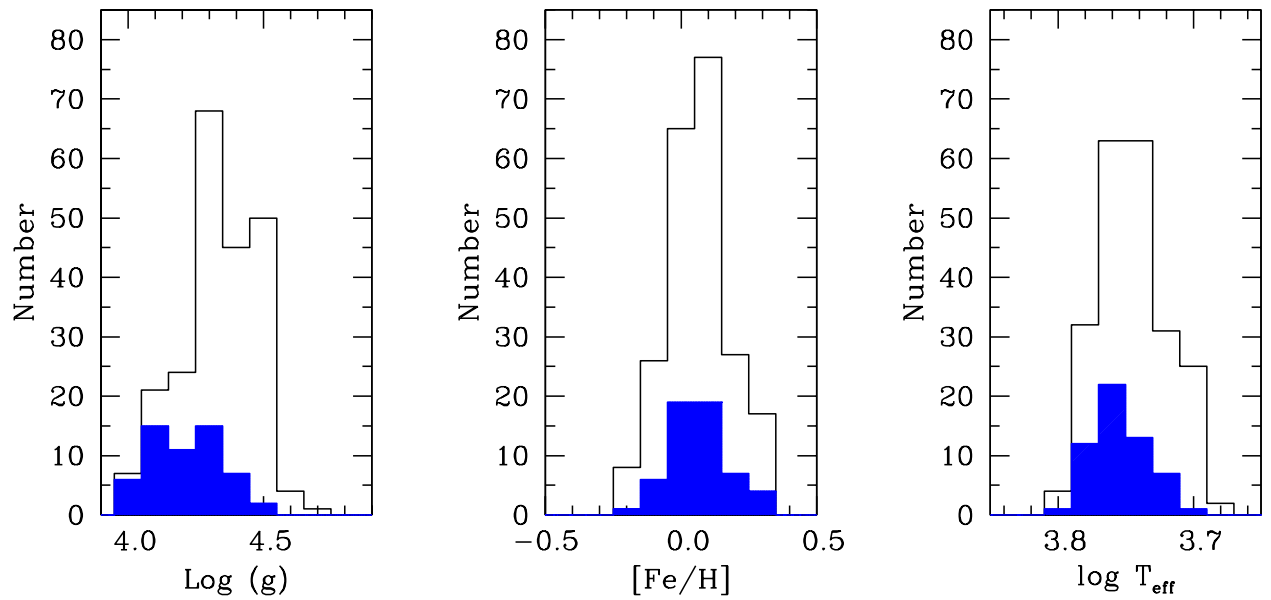


Fig. 9.— From left-to-right, the distribution of 220 stars as a function of  $\log(g)$ ,  $[\text{Fe}/\text{H}]$ , and  $T_{\text{eff}}$ . The solid blue inserts indicate the sub-sample with revised radii  $\geq 1.35$  times their KSAS radii. Again, this subsample tends have lower surface gravity and higher temperature than the full sample. There is no obvious difference in the  $[\text{Fe}/\text{H}]$  distribution of these two samples. (The data used to create this figure are available in the online journal.)

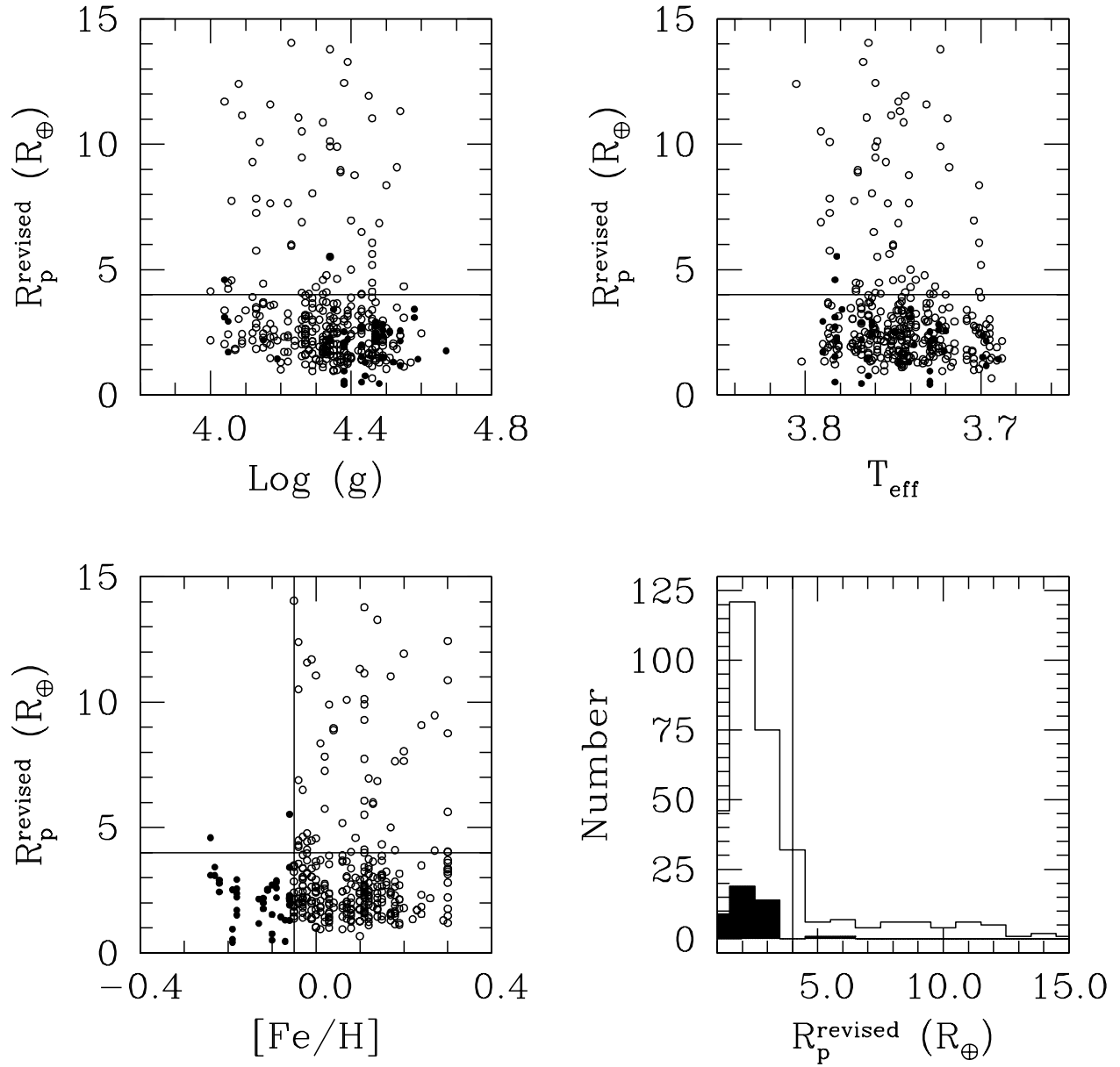


Fig. 10.— The top panels and the lower left panel compare revised exoplanet candidate radii (units:  $R_\oplus$ ) to host star characteristics. In all three panels, solid symbols correspond to exoplanet candidates associated with host stars with  $[\text{Fe}/\text{H}] \leq -0.05$  while open symbols correspond to stars with higher metallicity. Radii distributions for exoplanets orbiting lower metallicity stars ( $[\text{Fe}/\text{H}] \leq -0.05$ ) (solid histogram) and solar or greater metallicities (open histogram) are compared in the lower right panel. Exoplanet candidates with  $R_p^{\text{revised}} \geq 4R_\oplus$  are found at all temperatures and luminosities but are preferentially associated with stars of higher metallicity, in agreement with conclusions of Buchhave et al. (2012). (The data used to create this figure are available in the online journal.)

Table 1. Test star spectral fits

ID	Stellar properties from the literature						Values from this work			Difference in values			reference
	T <sub>eff</sub>	err	log(g)	err	[Fe/H]	err	T <sub>eff</sub>	log(g)	[Fe/H]	$\Delta T_{\text{eff}}$	$\Delta \log(g)$	$\Delta [\text{Fe}/\text{H}]$	
BD+05 3640	5104	44	4.85	0.06	-1.14	0.03	5079	4.01	-1.34	-25	-0.842	-0.196	Valenti & Fischer (2005)
HAT-P-2 <sup>a</sup>	6290	110	4.21	0.09	0.12	0.08	6274	3.77	0.04	-16	-0.440	-0.080	Bakos et al. (2007)
HAT-P-3 <sup>a</sup>	5185	46	4.58	0.04	0.27	0.04	5072	3.95	0.49	-113	-0.630	0.220	Torres et al. (2007)
HAT-P-4 <sup>a</sup>	5860	80	4.14	0.04	0.24	0.08	5787	3.42	0.25	-73	-0.720	0.010	Kovacs et al. (2007)
HAT-P-6 <sup>a</sup>	6570	80	4.22	0.03	-0.13	0.08	6487	3.97	-0.30	-83	-0.250	-0.170	Noyes et al. (2008)
HAT-P-8 <sup>a</sup>	6200	80	4.15	0.03	0.01	0.08	6073	3.25	-0.10	-127	-0.900	-0.110	Latham et al. (2009)
HAT-P-10 <sup>a</sup>	4980	60	4.56	0.02	0.13	0.08	4954	4.58	0.17	-26	0.020	0.040	Bakos et al. (2009a)
HAT-P-12	4591	60	4.61	0.01	-0.36	0.04	4391	4.21	-0.36	-200	-0.400	0.000	Hartman et al. (2009)
HAT-P-13 <sup>a</sup>	5653	90	4.13	0.04	0.41	0.08	5639	4.15	0.50	-14	0.020	0.090	Bakos et al. (2009b)
HAT-P-14 <sup>a</sup>	6600	90	4.25	0.03	0.11	0.08	6432	4.51	-0.16	-168	0.260	-0.270	Torres et al. (2010)
HAT-P-16 <sup>a</sup>	6158	80	4.34	0.03	0.17	0.08	6005	3.88	0.16	-153	-0.460	-0.010	Buchhave et al. (2010)
HAT-P-18 <sup>a</sup>	4803	80	4.57	0.04	0.10	0.08	4857	4.72	-0.05	54	0.150	-0.150	Hartman et al. (2011a)
HAT-P-19 <sup>a</sup>	4990	130	4.54	0.05	0.23	0.08	5010	4.47	0.40	20	-0.070	0.170	Hartman et al. (2011a)
HAT-P-20	4595	80	4.63	0.02	0.35	0.08	4315	3.71	-0.02	-280	-0.920	-0.370	Bakos et al. (2011)
HAT-P-21 <sup>a</sup>	5588	80	4.33	0.06	0.01	0.08	5544	3.86	0.10	-44	-0.470	0.090	Bakos et al. (2011)
HAT-P-22 <sup>a</sup>	5302	80	4.36	0.04	0.24	0.08	5284	3.96	0.45	-18	-0.400	0.210	Bakos et al. (2011)
HAT-P-25 <sup>a</sup>	5500	80	4.48	0.04	0.31	0.08	5478	4.08	0.50	-22	-0.400	0.190	Quinn et al. (2012)
HAT-P-26 <sup>a</sup>	5079	88	4.56	0.06	-0.04	0.08	5029	4.25	0.06	-50	-0.310	0.100	Hartman et al. (2011b)
HAT-P-27 <sup>a</sup>	5300	90	4.51	0.04	0.29	0.10	5314	4.25	0.50	14	-0.260	0.210	Béky et al. (2011)
HAT-P-28 <sup>a</sup>	5680	90	4.36	0.06	0.12	0.08	5586	3.83	0.25	-94	-0.530	0.130	Buchhave et al. (2011)
HAT-P-29 <sup>a</sup>	6087	88	4.34	0.06	0.21	0.08	5943	4.09	0.31	-144	-0.250	0.100	Buchhave et al. (2011)
HD3411	4657	100	2.59	0.10	0.31	0.17	4867	2.33	0.22	210	-0.260	-0.090	Luck & Heiter (2007)
HD7578	4715	100	2.64	0.10	0.24	0.17	4914	3.14	0.50	199	0.500	0.260	Luck & Heiter (2007)
HD8599	4957	100	3.11	0.10	-0.18	0.17	5022	2.66	0.06	65	-0.450	0.240	Luck & Heiter (2007)
HD23596 <sup>a</sup>	5903	44	3.97	0.06	0.22	0.03	5783	3.49	0.26	-120	-0.480	0.040	Valenti & Fischer (2005)
HD172310 <sup>a</sup>	5414	44	4.60	0.06	-0.42	0.03	5417	4.72	-0.58	3	0.120	-0.160	Valenti & Fischer (2005)
HD199442	4605	100	2.49	0.10	0.19	0.17	4777	2.34	0.17	172	-0.150	-0.020	Luck & Heiter (2007)
HD201891	5688	44	4.39	0.06	-1.12	0.03	5760	3.08	-1.13	72	-1.310	-0.010	Valenti & Fischer (2005)
HD204642	4733	100	2.90	0.10	0.08	0.17	4966	3.31	0.30	233	0.410	0.220	Luck & Heiter (2007)
HD210752	5835	44	4.37	0.06	-0.64	0.03	5761	3.36	-0.68	-74	-1.010	-0.040	Valenti & Fischer (2005)
HD211607	4992	100	3.17	0.10	0.13	0.17	5039	3.14	0.19	47	-0.030	0.060	Luck & Heiter (2007)
HD213619 <sup>a</sup>	7000	100	4.29	0.10	0.04	0.17	6750	4.10	-0.61	-250	-0.190	-0.650	Luck & Heiter (2007)
HD216259	4969	44	4.81	0.06	-0.63	0.03	4793	4.16	-0.93	-176	-0.650	-0.300	Valenti & Fischer (2005)
HD219615	5003	100	2.83	0.10	-0.52	0.17	4923	1.99	-0.58	-80	-0.840	-0.060	Luck & Heiter (2007)



Table 1—Continued

ID	Stellar properties from the literature						Values from this work			Difference in values			reference
	$T_{\text{eff}}$	err	$\log(g)$	err	[Fe/H]	err	$T_{\text{eff}}$	$\log(g)$	[Fe/H]	$\Delta T_{\text{eff}}$	$\Delta \log(g)$	$\Delta [\text{Fe}/\text{H}]$	
HD223869	4957	100	3.31	0.10	-0.02	0.17	5005	3.25	0.16	48	-0.060	0.180	Luck & Heiter (2007)
Kepler-9 <sup>a</sup>	5777	61	4.49	0.09	0.12	0.04	5763	4.00	-0.07	-14	-0.490	-0.190	Holman et al. (2010)
Kepler-16	4450	150	4.65	0.00	-0.30	0.20	4062	3.45	-0.55	-388	-1.200	-0.250	Doyle et al. (2011)
Kepler-21 <sup>a</sup>	6131	44	4.00	0.10	-0.15	0.06	5928	3.25	-0.20	-203	-0.750	-0.050	Howell et al. (2012)
KOI245 <sup>a</sup>	5369	44	4.57	0.01	-0.34	0.04	5241	4.33	-0.55	-128	-0.240	-0.210	Barclay et al. (2012)
KIC1432587	4165	65	1.66	0.01	-0.02	0.18	4709	2.32	-0.18	544	0.660	-0.160	Kallinger et al. (2012)
KIC10777816	4893	64	3.27	0.00	-0.22	0.18	5020	2.86	-0.10	127	-0.410	0.120	Kallinger et al. (2012)
KIC12306763	4153	71	1.83	0.01	-0.23	0.18	4729	2.32	0.22	576	0.490	0.450	Kallinger et al. (2012)
KIC12470054	4830	79	3.15	0.00	-0.29	0.18	4961	3.24	0.36	131	0.090	0.650	Kallinger et al. (2012)
KIC12506577	4418	74	2.20	0.01	0.18	0.18	4735	2.22	-0.48	317	0.020	-0.660	Kallinger et al. (2012)

<sup>a</sup>Star is one of 24 used to calibrate the model fits (see §5.5)

Table 2. Stellar properties determined for KOIs

KOI	Kepler ID	$m_{\text{Kep}}$ (mag.)	$T_{\text{eff}}^1$ (K)	$\log(g)^2$ (cgs)	$[\text{Fe}/\text{H}]^3$	$R_{\star}^4$ ( $R_{\odot}$ )	notes
13	9941662	9.958	...	...	...	...	b
13	9941662	9.958	...	...	...	...	b
14	7684873	10.470	...	...	...	...	bg
14	7684873	10.470	...	...	...	...	bg
70	6850504	12.498	5562	4.32	0.12	1.13	
74	6889235	10.960	...	...	...	...	bg
115	9579641	12.791	6065	4.43	-0.10	1.08	
136	7601633	13.439	6035	4.36	0.01	...	g
136	7601633	13.439	6001	4.37	0.11	...	g
149	3835670	13.397	5622	4.06	0.00	1.49	
161	5084942	13.341	4975	4.48	0.16	0.84	
183	9651668	14.290	5664	4.28	0.00	1.14	
184	7972785	14.933	6344	4.39	0.08	...	g
184	7972785	14.933	6121	4.12	-0.03	...	g
187	7023960	14.857	5786	4.40	0.30	1.11	f
191	5972334	14.991	5576	4.54	0.10	0.90	
196	9410930	14.465	5749	4.38	0.30	1.18	f
197	2987027	14.018	5020	4.50	0.01	0.84	
199	10019708	14.879	5932	4.05	0.13	...	g
201	6849046	14.014	5504	4.41	0.30	1.03	f
209	10723750	14.274	6185	4.26	-0.04	1.36	
209	10723750	14.274	6316	4.65	0.09	1.36	f
211	10656508	14.989	5822	4.25	-0.00	1.26	
216	6152974	14.711	5056	4.40	0.12	0.90	
222	4249725	14.735	4750	4.47	-0.19	...	
223	4545187	14.708	...	...	...	...	e
224	5547480	14.782	5742	4.26	0.01	...	g
225	5801571	14.784	6362	4.36	-0.00	1.26	
232	4833421	14.247	6058	4.34	-0.06	1.15	
232	4833421	14.247	6062	4.48	-0.00	1.15	
238	7219825	14.061	6095	4.17	-0.04	1.49	
245	8478994	9.705	5359	4.38	-0.19	0.97	
251	10489206	14.752	...	...	...	...	a
260	8292840	10.500	6161	4.05	-0.18	1.53	
265	12024120	11.994	5915	4.07	0.06	1.64	
269	7670943	10.927	6162	4.04	-0.03	1.98	
271	9451706	11.485	5919	4.12	0.13	...	g
273	3102384	11.457	5586	4.35	0.20	1.05	
286	8258171	11.641	...	...	...	...	bg
286	8258171	11.641	...	...	...	...	bg
326	9880467	12.960	...	...	...	...	d
350	11395587	13.387	5656	4.29	0.01	1.14	
353	11566064	13.374	6382	4.08	-0.04	1.77	
355	11621223	13.174	5930	4.08	0.13	1.56	
360	12107021	13.021	...	...	...	...	c
361	12404954	13.100	5562	4.39	0.08	1.03	
364	7296438	10.087	5798	4.15	0.30	...	fg
368	6603043	11.375	...	...	...	...	b
372	6471021	12.391	5735	4.36	-0.01	1.13	
372	6471021	12.391	5753	4.36	0.07	1.13	
377	3323887	13.803	5830	4.31	0.00	1.09	
377	3323887	13.803	5932	4.43	0.08	1.09	
383	3342463	13.109	5994	4.30	-0.02	...	g
384	3353050	13.281	6105	4.15	0.02	1.49	

Table 2—Continued

KOI	Kepler ID	$m_{\text{Kep}}$ (mag.)	$T_{\text{eff}}^1$ (K)	$\log(g)^2$ (cgs)	$[\text{Fe}/\text{H}]^3$	$R_{\star}^4$ ( $R_{\odot}$ )	notes
387	3733628	13.577	...	...	...	...	a
389	3847708	13.936	5222	4.38	0.30	...	fg
391	3858804	13.778	5174	4.27	0.07	...	g
397	4376644	13.767	6095	4.36	-0.04	...	g
398	9946525	15.342	5225	4.53	0.24	0.87	f
406	5035972	14.385	6072	4.53	0.30	...	fg
406	5035972	14.385	5803	4.19	0.20	...	g
406	5035972	14.385	5824	4.27	0.15	...	g
433	10937029	14.924	5096	4.30	0.09	...	
448	5640085	14.902	...	...	...	...	af
456	7269974	14.619	5538	4.33	0.18	1.04	
471	10019643	14.415	5389	4.31	0.07	1.11	
474	10460984	14.282	5812	4.27	-0.02	1.27	
495	4049108	14.873	...	...	...	...	dg
497	4757437	14.606	5946	4.31	0.12	1.29	
498	4833135	14.660	6157	4.34	-0.20	...	g
501	4951877	14.612	5772	4.33	0.08	1.09	
504	5461440	14.560	...	...	...	...	e
508	6266741	14.387	5540	4.39	0.30	1.01	f
509	6381846	14.883	5454	4.45	0.16	0.98	
518	8017703	14.287	...	...	...	...	a
520	8037145	14.550	4963	4.43	0.08	...	g
523	8806123	15.000	5766	4.43	-0.03	0.98	
528	9941859	14.598	5377	4.29	-0.00	1.08	
530	10266615	14.909	...	...	...	...	d
536	10965008	14.499	5458	4.26	0.15	1.14	
536	10965008	14.499	5555	4.32	0.16	1.14	
537	11073351	14.665	5832	4.36	0.12	1.14	
543	11823054	14.707	5037	4.32	-0.05	...	
548	12600735	14.020	6011	4.35	-0.06	1.15	
551	4270253	14.943	5577	4.26	0.09	1.17	
555	5709725	14.759	5199	4.42	0.12	0.92	
555	5709725	14.759	5242	4.44	0.10	0.92	
561	6665695	14.005	4996	4.27	-0.03	...	
563	6707833	14.519	5770	4.18	0.00	1.35	
564	6786037	14.854	5754	4.26	0.27	1.32	f
568	7595157	14.140	5294	4.32	0.01	1.09	
569	8008206	14.458	4982	4.54	-0.13	0.71	
571	8120608	14.625	...	...	...	...	a
572	8193178	14.173	5854	4.06	-0.04	...	
573	8344004	14.674	5621	4.35	0.07	1.08	
574	8355239	14.859	4956	4.43	-0.03	0.86	
582	9020160	14.808	5101	4.47	0.09	...	g
583	9076513	14.573	5570	4.18	0.17	1.41	
589	9763754	14.547	5863	4.48	-0.07	1.03	
590	9782691	14.615	5880	4.15	-0.02	1.59	
591	9886221	14.396	5497	4.23	0.19	...	g
594	10216045	14.736	5268	4.51	-0.10	...	g
597	10600261	14.915	5564	4.12	-0.03	1.46	
622	12417486	14.932	...	...	...	...	d
636	5090690	13.252	6606	4.68	-0.11	...	fg
644	5356593	13.725	5731	4.29	-0.03	...	g
649	5613330	13.310	6036	4.14	0.12	1.59	
650	5786676	13.594	5054	4.47	0.02	0.90	

Table 2—Continued

KOI	Kepler ID	$m_{\text{Kep}}$ (mag.)	$T_{\text{eff}}^1$ (K)	$\log(g)^2$ (cgs)	$[\text{Fe}/\text{H}]^3$	$R_{\star}^4$ ( $R_{\odot}$ )	notes
671	7040629	13.749	6040	4.33	0.03	1.19	
680	7529266	13.643	6116	4.14	0.07	1.48	
681	7598128	13.204	6117	4.03	0.01	...	g
692	8557374	13.648	5541	4.30	0.14	1.10	
693	8738735	13.949	...	...	...	...	c
694	8802165	13.939	5578	4.35	0.13	1.10	
709	9578686	13.940	5330	4.39	-0.18	0.89	
710	9590976	13.294	...	...	...	...	c
711	9597345	13.967	5501	4.39	0.30	1.05	f
712	9640976	13.720	5501	4.55	0.02	...	g
717	9873254	13.387	5522	4.27	0.26	1.26	f
730	10227020	15.344	5812	4.27	0.15	1.27	
733	10271806	15.644	5100	4.46	-0.03	0.86	
736	10340423	15.962	...	...	...	...	a
738	10358759	15.282	5497	4.58	-0.23	0.82	
749	10601284	15.416	5187	4.38	0.10	1.00	
752	10797460	15.347	5457	4.47	0.12	0.89	
757	10910878	15.841	5025	4.46	0.11	0.89	
767	11414511	15.052	5530	4.45	0.20	0.93	
780	11918099	15.334	5007	4.60	0.10	0.75	
787	12366084	15.367	5718	4.43	0.30	1.05	f
794	2713049	15.026	5523	4.35	-0.04	1.07	
801	3351888	15.001	5541	4.32	0.30	1.24	f
806	3832474	15.403	5285	4.34	0.11	0.98	
812	4139816	15.954	...	...	...	...	a
824	5164255	16.422	4976	4.36	0.04	...	
825	5252423	15.289	...	...	...	...	a
829	5358241	15.386	5779	4.40	0.03	1.09	
837	5531576	15.660	4754	4.39	0.20	...	
840	5651104	15.028	5236	4.56	0.19	...	g
841	5792202	15.855	5036	4.23	0.06	...	
842	5794379	15.389	...	...	...	...	a
844	6022556	15.581	5726	4.46	-0.01	0.99	
847	6191521	15.201	5511	4.22	0.20	1.22	
860	6680177	15.245	...	...	...	...	d
861	6685526	15.001	5262	4.67	-0.12	0.72	f
864	6849310	15.604	5524	4.48	0.09	...	g
865	6862328	15.085	5456	4.34	0.07	...	g
865	6862328	15.085	5551	4.47	0.00	...	g
873	7118364	15.024	5756	4.34	0.13	1.15	
874	7134976	15.024	4978	4.47	0.17	0.84	
877	7287995	15.019	...	...	...	...	a
881	7373451	15.859	5011	4.46	0.06	0.85	
885	7436215	15.161	5045	4.22	0.13	...	
896	7825899	15.258	5327	4.55	0.15	0.84	
897	7849854	15.257	5851	4.39	0.14	1.10	
905	8180063	15.289	5874	4.30	0.01	...	g
906	8226994	15.460	5028	4.50	0.00	0.80	
912	8505670	15.058	...	...	...	...	a
918	8672910	15.011	5231	4.46	0.17	0.91	
934	9334289	15.843	5558	4.36	-0.03	1.07	
935	9347899	15.237	6106	4.13	0.02	1.58	
938	9415172	15.596	5331	4.32	0.30	1.10	f
939	9466668	15.065	5540	4.46	0.18	0.92	

Table 2—Continued

KOI	Kepler ID	$m_{\text{Kep}}$ (mag.)	$T_{\text{eff}}^1$ (K)	$\log(g)^2$ (cgs)	[Fe/H] <sup>3</sup>	$R_{\star}^4$ ( $R_{\odot}$ )	notes
943	9513865	15.733	5046	4.35	0.19	0.96	
945	9605514	15.083	...	...	...	...	c
947	9710326	15.190	...	...	...	...	a
962	8846163	14.005	...	...	...	...	a
974	9414417	9.582	...	...	...	...	c
994	1431122	14.613	5294	4.32	0.23	1.17	f
998	1432214	15.661	5804	4.15	0.11	1.53	
1015	8158127	14.500	5898	4.00	-0.02	1.70	
1032	2162635	13.862	5008	4.18	0.14	...	
1052	5956342	15.381	5930	4.27	-0.01	1.19	
1053	5956656	15.376	5552	4.32	0.23	1.10	f
1059	6060203	14.803	5365	4.37	0.08	1.01	
1067	8246781	14.685	6031	4.24	-0.11	1.18	
1069	8222813	15.070	5075	4.42	0.19	0.87	
1085	10118816	15.233	...	...	...	...	a
1089	3247268	14.696	5743	4.34	0.11	1.11	
1096	3230491	14.709	5520	4.69	-0.11	...	f
1099	2853093	15.435	5779	4.29	0.20	1.18	
1102	3231341	14.925	5897	4.05	-0.04	1.70	
1106	3240158	14.818	6046	4.36	0.00	1.11	
1152	10287248	13.987	...	...	...	...	ag
1161	10426656	14.678	5330	4.36	-0.00	1.02	
1163	10468940	14.968	5354	4.38	-0.06	1.05	
1164	10341831	14.960	...	...	...	...	ag
1174	10287723	13.447	...	...	...	...	a
1198	3447722	15.319	6125	4.15	0.06	1.48	
1203	3962243	15.368	5781	4.47	-0.22	0.95	
1208	3962440	13.594	6404	4.35	-0.03	...	
1210	3962357	14.377	6136	4.17	0.10	...	
1219	3440861	14.463	4945	4.46	0.10	0.83	
1226	6621116	15.324	5304	4.21	0.30	1.22	f
1239	6607286	15.005	5639	4.24	-0.04	1.20	
1240	6690082	14.466	5535	4.34	0.14	1.06	
1261	8678594	15.120	5587	4.04	-0.01	1.55	
1268	8813698	14.814	5804	4.23	-0.05	1.27	
1276	8804283	14.766	5435	4.44	0.08	0.99	
1276	8804283	14.766	5478	4.36	0.26	0.99	f
1278	8609450	15.204	5857	4.47	-0.09	1.01	
1288	10790387	15.128	...	...	...	...	c
1301	10538176	15.824	5294	4.49	-0.09	0.90	
1305	10730034	15.173	5108	4.37	0.03	0.94	
1306	10858691	15.587	5812	4.45	-0.05	1.02	
1307	10973814	14.775	5514	4.34	0.15	1.02	
1312	10963242	14.706	6111	4.29	0.08	1.29	
1337	4243911	14.829	5194	4.57	0.29	0.87	f
1355	7211141	15.897	5673	4.12	0.11	1.52	
1360	7102227	15.596	...	...	...	...	a
1364	6962977	15.956	5269	4.43	0.11	0.90	
1367	6934291	15.055	5070	4.48	-0.00	0.85	
1376	6774826	13.997	...	...	...	...	b
1396	9455556	15.843	5626	4.60	0.13	...	
1407	9007866	15.755	5270	4.35	0.06	1.03	
1408	9150827	14.688	...	...	...	...	a
1423	11177707	15.740	5023	4.18	0.12	...	

Table 2—Continued

KOI	Kepler ID	$m_{\text{Kep}}$ (mag.)	$T_{\text{eff}}^1$ (K)	$\log(g)^2$ (cgs)	$[\text{Fe}/\text{H}]^3$	$R_{\star}^4$ ( $R_{\odot}$ )	notes
1425	11254382	15.269	5630	4.28	0.12	1.21	
1429	11030711	15.531	5644	4.46	0.30	1.01	f
1432	11014932	15.017	5525	4.35	0.07	1.01	
1434	11493431	14.782	4787	4.45	0.19	...	
1439	11027624	12.849	5913	4.06	0.11	1.64	
1472	7761545	15.061	5582	4.48	0.14	0.93	
1475	4770365	15.937	...	...	...	...	a
1480	7512982	15.887	4859	4.29	-0.15	...	
1483	11909686	14.305	5850	4.26	0.29	1.30	f
1503	12400538	14.827	5628	4.19	0.13	1.21	
1503	12400538	14.827	5531	4.27	0.13	1.21	
1515	7871954	14.390	...	...	...	...	a
1527	7768451	14.879	5358	4.28	0.08	1.14	
1557	5371776	14.840	...	...	...	...	a
1564	5184584	15.287	...	...	...	...	c
1567	5438099	15.565	4960	4.47	-0.03	0.84	
1574	10028792	14.600	5641	4.09	0.11	1.59	
1582	4918309	15.402	5381	4.17	-0.02	1.36	
1588	5617854	14.699	...	...	...	...	a
1589	5301750	14.764	5866	4.13	-0.05	1.43	
1590	5542466	15.674	4906	4.47	-0.05	0.81	
1596	10027323	15.157	...	...	...	...	a
1601	5438757	14.659	5535	4.34	-0.01	1.06	
1611	12644769	11.762	...	...	...	...	a
1613	6268648	11.049	...	...	...	...	c
1614	10514429	11.413	5792	4.19	-0.05	1.33	
1627	6543893	15.767	6070	4.04	-0.24	1.64	
1636	10621666	14.598	5858	4.35	-0.10	...	g
1641	10879038	14.971	5776	4.50	0.12	0.97	
1646	11046025	14.293	...	...	...	...	a
1647	11153121	14.167	5687	4.29	0.19	1.17	
1649	11337141	14.963	...	...	...	...	a
1688	6310636	14.542	5846	4.07	0.13	1.51	
1720	10015937	15.742	5246	4.54	-0.18	0.75	
1739	7199906	15.129	5592	4.10	0.08	1.51	
1750	6209677	14.800	5450	4.48	0.17	0.89	
1820	8277797	13.530	5402	4.45	0.10	0.90	
1849	9735426	14.624	5271	4.49	0.11	0.89	
1858	8160953	14.767	5395	4.33	-0.02	1.06	
1860	4157325	14.028	5666	4.27	0.11	1.14	
1866	9520838	14.986	5462	4.32	0.09	1.09	
1867	8167996	15.018	...	...	...	...	a
1874	8978528	15.434	...	...	...	...	a
1882	6205228	14.668	5711	4.27	0.14	1.26	
1891	8680979	15.261	4879	4.47	0.15	0.81	
1895	4263293	15.862	...	...	...	...	a
1900	9353314	14.744	...	...	...	...	a
1902	5809954	14.645	...	...	...	...	a
1908	5706966	14.731	...	...	...	...	a
1922	9411166	15.356	5739	4.33	0.11	1.20	
1931	10978763	14.531	5348	4.32	0.01	1.10	
1934	4242147	14.649	...	...	...	...	a
1940	10005788	15.389	...	...	...	...	a
1945	11656918	14.520	5098	4.21	0.15	...	

Table 2—Continued

KOI	Kepler ID	$m_{\text{Kep}}$ (mag.)	$T_{\text{eff}}^1$ (K)	$\log(g)^2$ (cgs)	$[\text{Fe}/\text{H}]^3$	$R_{\star}^4$ ( $R_{\odot}$ )	notes
1952	7747425	14.601	5617	4.33	0.03	1.17	
1974	7289577	14.937	5363	4.36	0.07	1.00	
1992	11450414	14.513	5589	4.12	-0.02	1.40	
2006	10525027	14.220	...	...	...	...	a
2022	8564674	14.746	5744	4.49	0.14	0.96	
2025	4636578	13.781	...	...	...	...	c
2031	5940165	14.796	...	...	...	...	a
2038	8950568	14.779	5375	4.22	0.11	1.24	
2044	9656252	15.818	5788	4.47	0.30	1.04	f
2051	7265298	15.087	5740	4.38	-0.01	1.11	
2057	9573685	15.026	...	...	...	...	a
2066	3239671	14.904	5494	4.30	-0.04	1.17	
2073	8164257	15.565	4944	4.40	0.09	...	
2083	7097965	13.516	5875	4.21	0.24	1.35	f
2087	6922710	11.863	5902	4.22	0.08	1.37	
2095	7918992	14.691	5805	4.40	0.06	1.11	
2103	7620413	14.736	5579	4.39	0.08	0.98	
2111	8612275	14.866	5467	4.49	0.11	0.93	
2114	6921944	15.180	...	...	...	...	a
2115	9532052	16.144	5065	4.32	0.02	...	
2116	8164012	14.690	5909	4.05	-0.00	1.69	
2121	9415108	14.979	5362	4.33	0.08	1.01	
2132	9661979	14.552	...	...	...	...	c
2147	10404582	14.500	5758	4.43	0.06	1.01	
2160	5546761	14.874	5792	4.26	-0.05	1.18	
2164	7204981	15.162	5361	4.40	0.00	0.93	
2168	11308499	14.842	5857	4.34	-0.03	1.18	
2171	11410904	14.972	5772	4.51	0.17	0.97	
2177	10965588	15.481	5041	4.41	0.02	0.89	
2200	10909127	15.353	5438	4.69	-0.10	...	f
2209	8168187	14.310	...	...	...	...	c
2210	4142847	15.195	4895	4.59	-0.08	0.71	
2215	7050060	12.999	6063	4.27	0.03	1.36	
2218	12058204	14.514	5589	4.33	0.14	1.05	
2220	6871071	14.686	5638	4.09	0.12	1.59	
2224	8892157	14.966	5710	4.49	0.08	0.94	
2238	8229458	14.634	...	...	...	...	a
2247	7802719	14.374	...	...	...	...	a
2248	11030475	15.498	5107	4.31	0.02	...	
2261	3734418	14.110	5064	4.35	0.08	0.95	
2282	6751874	14.207	5867	4.15	-0.06	1.46	
2286	8973129	15.056	5466	4.43	-0.12	0.87	
2294	6934986	14.895	5585	4.18	0.30	1.41	f
2296	11498128	14.552	5534	4.25	-0.00	1.21	
2307	7661065	14.854	5292	4.52	0.07	0.83	
2310	11718144	14.640	5477	4.52	0.07	0.88	
2317	10684670	14.285	5559	4.38	0.30	1.07	f
2318	11495458	14.471	...	...	...	...	a
2319	9003401	13.355	6059	4.28	0.07	1.30	
2320	10481045	15.047	5758	4.69	-0.07	...	fg
2347	8235924	14.934	...	...	...	...	a
2373	10798331	14.685	5566	4.27	0.18	1.18	
2383	9395024	15.133	5654	4.28	0.08	1.25	
2392	7382313	14.985	5574	4.44	-0.06	0.93	

Table 2—Continued

KOI	Kepler ID	$m_{\text{Kep}}$ (mag.)	$T_{\text{eff}}^1$ (K)	$\log(g)^2$ (cgs)	$[\text{Fe}/\text{H}]^3$	$R_{\star}^4$ ( $R_{\odot}$ )	notes
2393	4665571	14.903	4815	4.45	-0.06	...	
2399	11461433	14.100	5073	4.32	-0.00	...	
2401	10336951	14.847	...	...	...	...	a
2407	12120484	14.150	5935	4.26	0.18	1.35	
2410	8676038	15.141	5615	4.51	-0.11	0.90	
2413	3234598	15.070	...	...	...	...	a
2417	9654468	16.220	...	...	...	...	a
2420	7107802	14.746	5559	4.29	0.11	1.14	
2421	8838950	14.363	...	...	...	...	d
2430	3533469	14.338	5405	4.43	0.02	0.99	
2433	11968463	15.212	...	...	...	...	c
2437	5036705	14.725	6150	4.21	0.10	1.38	
2459	8572936	14.875	5805	4.44	-0.10	1.02	
2460	11236244	15.006	...	...	...	...	a
2466	8544992	14.993	...	...	...	...	a
2469	6149910	15.048	...	...	...	...	a
2509	9880190	15.035	5001	4.39	0.02	0.92	
2517	8947520	14.511	5589	4.59	-0.09	...	
2521	7183745	15.860	4999	4.49	-0.18	0.77	
2535	9635606	14.985	4814	4.34	0.02	...	
2543	12469800	15.351	4945	4.48	-0.02	0.80	
2548	9580167	14.992	...	...	...	...	a
2552	8757824	14.460	6081	4.30	-0.01	1.21	
2554	10471621	15.439	...	...	...	...	a
2571	6867588	14.434	5215	4.55	0.19	0.82	
2597	12120307	14.790	...	...	...	...	c
2600	9777251	15.053	5497	4.36	0.16	...	g
2601	7531677	13.915	5865	4.20	0.00	1.32	
2624	8429314	15.174	5798	4.33	0.01	1.12	
2627	6124512	14.667	...	...	...	...	d
2628	10070468	14.812	5824	4.19	-0.08	1.32	
2637	9574179	15.016	5694	4.29	0.01	1.22	
2658	8547429	14.406	5794	4.38	0.22	1.11	
2662	3426367	14.488	...	...	...	...	a
2691	4552729	14.981	...	...	...	...	a
2730	8415200	13.836	5582	4.20	0.03	1.25	
2762	8210018	15.028	...	...	...	...	a
2770	10917043	15.558	...	...	...	...	a
2820	11963206	15.273	5707	4.69	-0.08	...	f
2869	7767162	13.749	6334	4.22	0.15	1.36	
2920	7090524	14.455	5513	4.26	0.24	1.32	f
2931	8611257	14.699	4991	4.49	-0.03	0.85	
3255	8183288	14.352	...	...	...	...	a
3259	2853029	15.679	5314	4.47	-0.05	0.88	

<sup>1</sup>Uncertainty in  $T_{\text{eff}}$  is  $\pm 75$  K<sup>2</sup>Uncertainty in  $\log(g)$  is  $\pm 0.15$ <sup>3</sup>Uncertainty in  $[\text{Fe}/\text{H}]$  is  $\pm 0.10$ <sup>4</sup>Uncertainty in  $R_{\star}$  is  $\pm 0.05 R_{\odot}$ 

Note. — Values in the notes column flag the following conditions: (a)  $T_{\text{eff}} < 4750\text{K}$ ; (b)  $T_{\text{eff}} > 7200\text{K}$ ; (c)  $\log(g) < 4.00$  and  $5500\text{K} \leq T_{\text{eff}} \leq 7200\text{K}$ ; (d)  $\log(g) < 4.15$  and  $4750\text{K} \leq T_{\text{eff}} < 5500\text{K}$ ; (e)  $[\text{Fe}/\text{H}] < -0.25$ ; (f) model fit reached a parameters limit (g) Now known to be a false positive.



Table 3. Data used in Figures 8–10

Planet ID	Parent star (KIC ID)	$\log(T_{\text{eff}})$ (K)	$\log(g)$ (cgs)	[Fe/H]	$R_*$ ( $R_\odot$ )	$R_*^{\text{revised}}/R_*^{\text{KSAS}}$	$R_p$ ( $R_\oplus$ )
K00070.01	6850504	3.745	4.32	0.12	1.13	1.21	3.74
K00070.02	6850504	3.745	4.32	0.12	1.13	1.21	2.32
K00070.03	6850504	3.745	4.32	0.12	1.13	1.21	3.35
K00070.04	6850504	3.745	4.32	0.12	1.13	1.21	1.10
K00070.05	6850504	3.745	4.32	0.12	1.13	1.21	1.24
K00115.01	9579641	3.783	4.43	-0.10	1.08	0.81	2.71
K00115.02	9579641	3.783	4.43	-0.10	1.08	0.81	1.53
K00115.03	9579641	3.783	4.43	-0.10	1.08	0.81	0.51
K00149.01	3835670	3.750	4.06	0.00	1.49	0.83	4.57
K00161.01	5084942	3.697	4.48	0.16	0.84	1.05	2.82
K00183.01	9651668	3.753	4.28	0.00	1.14	1.31	15.20
K00187.01	7023960	3.762	4.40	0.30	1.11	1.17	17.16
K00191.01	5972334	3.746	4.54	0.10	0.90	1.06	11.32
K00191.02	5972334	3.746	4.54	0.10	0.90	1.06	2.38
K00191.03	5972334	3.746	4.54	0.10	0.90	1.06	1.27
K00191.04	5972334	3.746	4.54	0.10	0.90	1.06	2.36
K00196.01	9410930	3.760	4.38	0.30	1.18	1.26	12.44
K00197.01	2987027	3.701	4.50	0.01	0.84	1.07	8.36
K00201.01	6849046	3.741	4.41	0.30	1.03	0.88	8.76
K00209.01	10723750	3.791	4.26	-0.04	1.36	1.27	10.51
K00209.02	10723750	3.791	4.26	-0.04	1.36	1.27	6.89
K00211.01	10656508	3.765	4.25	-0.00	1.26	1.12	11.06
K00216.01	6152974	3.704	4.40	0.12	0.90	0.97	6.96
K00216.02	6152974	3.704	4.40	0.12	0.90	0.97	1.45
K00225.01	5801571	3.804	4.36	-0.00	1.26	1.45	58.88
K00232.01	4833421	3.782	4.34	-0.06	1.15	1.28	5.53
K00232.02	4833421	3.782	4.34	-0.06	1.15	1.28	2.22
K00232.03	4833421	3.782	4.34	-0.06	1.15	1.28	2.17
K00232.04	4833421	3.782	4.34	-0.06	1.15	1.28	2.29
K00232.05	4833421	3.782	4.34	-0.06	1.15	1.28	2.17
K00238.01	7219825	3.785	4.17	-0.04	1.49	1.48	3.56
K00238.02	7219825	3.785	4.17	-0.04	1.49	1.48	2.00
K00245.01	8478994	3.729	4.38	-0.19	0.97	1.26	2.52
K00245.02	8478994	3.729	4.38	-0.19	0.97	1.26	0.95
K00245.03	8478994	3.729	4.38	-0.19	0.97	1.26	0.42
K00245.04	8478994	3.729	4.38	-0.19	0.97	1.26	0.54
K00260.01	8292840	3.790	4.05	-0.18	1.53	1.11	1.71
K00260.02	8292840	3.790	4.05	-0.18	1.53	1.11	2.93
K00262.01	11807274	3.784	4.16	-0.01	1.49	0.94	2.07
K00262.02	11807274	3.784	4.16	-0.01	1.49	0.94	2.63
K00265.01	12024120	3.772	4.07	0.06	1.64	1.39	1.79
K00269.01	7670943	3.790	4.04	-0.03	1.98	1.38	2.03
K00273.01	3102384	3.747	4.35	0.20	1.05	0.98	1.79
K00350.01	11395587	3.753	4.29	0.01	1.14	1.07	2.52
K00353.01	11566064	3.805	4.08	-0.04	1.77	1.35	12.40
K00355.01	11621223	3.773	4.08	0.13	1.56	1.29	3.03
K00361.01	12404954	3.745	4.39	0.08	1.03	1.04	1.59
K00372.01	6471021	3.76	4.36	0.03	1.12	1.17	9.90
K00377.01	3323887	3.77	4.37	0.04	1.09	1.08	8.96
K00377.02	3323887	3.77	4.37	0.04	1.09	1.08	8.88
K00377.03	3323887	3.77	4.37	0.04	1.09	1.08	1.81
K00384.01	3353050	3.786	4.15	0.02	1.49	1.33	2.28
K00398.01	9946525	3.718	4.53	0.24	0.87	1.05	9.08
K00398.02	9946525	3.718	4.53	0.24	0.87	1.05	3.49

Table 3—Continued

Planet ID	Parent star (KIC ID)	$\log(T_{\text{eff}})$ (K)	$\log(g)$ (cgs)	[Fe/H]	$R_*$ ( $R_{\odot}$ )	$R_*^{\text{revised}}/R_*^{\text{KSAS}}$	$R_p$ ( $R_{\oplus}$ )
K00398.03	9946525	3.718	4.53	0.24	0.87	1.05	1.84
K00456.01	7269974	3.743	4.33	0.18	1.04	1.25	4.10
K00456.02	7269974	3.743	4.33	0.18	1.04	1.25	1.88
K00471.01	10019643	3.732	4.31	0.07	1.11	1.31	3.00
K00471.02	10019643	3.732	4.31	0.07	1.11	1.31	1.36
K00474.01	10460984	3.764	4.27	-0.02	1.27	1.23	3.20
K00474.02	10460984	3.764	4.27	-0.02	1.27	1.23	3.15
K00474.03	10460984	3.764	4.27	-0.02	1.27	1.23	3.97
K00497.01	4757437	3.774	4.31	0.12	1.29	1.26	3.46
K00497.02	4757437	3.774	4.31	0.12	1.29	1.26	1.93
K00501.01	4951877	3.761	4.33	0.08	1.09	1.23	2.74
K00508.01	6266741	3.744	4.39	0.30	1.01	0.98	3.37
K00508.02	6266741	3.744	4.39	0.30	1.01	0.98	3.24
K00509.01	6381846	3.737	4.45	0.16	0.98	1.21	2.71
K00509.02	6381846	3.737	4.45	0.16	0.98	1.21	3.24
K00523.01	8806123	3.761	4.43	-0.03	0.98	0.93	6.50
K00523.02	8806123	3.761	4.43	-0.03	0.98	0.93	2.67
K00528.01	9941859	3.731	4.29	-0.00	1.08	1.11	2.92
K00528.02	9941859	3.731	4.29	-0.00	1.08	1.11	3.65
K00528.03	9941859	3.731	4.29	-0.00	1.08	1.11	3.47
K00536.01	10965008	3.74	4.29	0.15	1.15	1.29	3.87
K00537.01	11073351	3.766	4.36	0.12	1.14	1.24	2.51
K00548.01	12600735	3.779	4.35	-0.06	1.15	1.10	3.41
K00551.01	4270253	3.746	4.26	0.09	1.17	1.34	3.00
K00551.02	4270253	3.746	4.26	0.09	1.17	1.34	2.66
K00555.01	5709725	3.72	4.43	0.11	0.92	1.02	1.43
K00555.02	5709725	3.72	4.43	0.11	0.92	1.02	2.72
K00563.01	6707833	3.761	4.18	0.00	1.35	1.45	2.60
K00564.01	6786037	3.760	4.26	0.27	1.32	1.55	4.08
K00564.02	6786037	3.760	4.26	0.27	1.32	1.55	9.47
K00568.01	7595157	3.724	4.32	0.01	1.09	1.38	1.86
K00569.01	8008206	3.697	4.54	-0.13	0.71	0.90	2.15
K00569.02	8008206	3.697	4.54	-0.13	0.71	0.90	1.17
K00573.01	8344004	3.750	4.35	0.07	1.08	1.02	3.06
K00573.02	8344004	3.750	4.35	0.07	1.08	1.02	1.76
K00574.01	8355239	3.695	4.43	-0.03	0.86	1.24	3.02
K00574.02	8355239	3.695	4.43	-0.03	0.86	1.24	1.40
K00583.01	9076513	3.746	4.18	0.17	1.41	1.51	2.32
K00590.01	9782691	3.769	4.15	-0.02	1.59	1.52	3.69
K00590.02	9782691	3.769	4.15	-0.02	1.59	1.52	4.44
K00597.01	10600261	3.745	4.12	-0.03	1.46	1.50	3.91
K00597.02	10600261	3.745	4.12	-0.03	1.46	1.50	2.18
K00649.01	5613330	3.781	4.14	0.12	1.59	1.36	3.15
K00650.01	5786676	3.704	4.47	0.02	0.90	1.19	2.76
K00671.01	7040629	3.781	4.33	0.03	1.19	1.20	1.99
K00671.02	7040629	3.781	4.33	0.03	1.19	1.20	1.62
K00671.03	7040629	3.781	4.33	0.03	1.19	1.20	1.93
K00680.01	7529266	3.786	4.14	0.07	1.48	1.40	10.09
K00692.01	8557374	3.744	4.30	0.14	1.10	1.32	1.45
K00692.02	8557374	3.744	4.30	0.14	1.10	1.32	2.66
K00694.01	8802165	3.746	4.35	0.13	1.10	1.31	3.64
K00709.01	9578686	3.727	4.39	-0.18	0.89	1.09	2.22
K00711.01	9597345	3.740	4.39	0.30	1.05	0.99	3.15
K00711.02	9597345	3.740	4.39	0.30	1.05	0.99	1.48

Table 3—Continued

Planet ID	Parent star (KIC ID)	$\log(T_{\text{eff}})$ (K)	$\log(g)$ (cgs)	[Fe/H]	$R_*$ ( $R_{\odot}$ )	$R_*^{\text{revised}}/R_*^{\text{KSAS}}$	$R_p$ ( $R_{\oplus}$ )
K00711.03	9597345	3.740	4.39	0.30	1.05	0.99	2.80
K00717.01	9873254	3.742	4.27	0.26	1.26	1.17	2.18
K00730.01	10227020	3.764	4.27	0.15	1.27	1.29	3.68
K00730.02	10227020	3.764	4.27	0.15	1.27	1.29	2.44
K00730.03	10227020	3.764	4.27	0.15	1.27	1.29	3.14
K00730.04	10227020	3.764	4.27	0.15	1.27	1.29	2.02
K00733.01	10271806	3.708	4.46	-0.03	0.86	1.33	3.39
K00733.02	10271806	3.708	4.46	-0.03	0.86	1.33	2.95
K00733.03	10271806	3.708	4.46	-0.03	0.86	1.33	1.81
K00733.04	10271806	3.708	4.46	-0.03	0.86	1.33	3.04
K00738.01	10358759	3.740	4.58	-0.23	0.82	0.96	3.42
K00738.02	10358759	3.740	4.58	-0.23	0.82	0.96	3.09
K00749.01	10601284	3.715	4.38	0.10	1.00	1.32	2.93
K00749.02	10601284	3.715	4.38	0.10	1.00	1.32	2.06
K00749.03	10601284	3.715	4.38	0.10	1.00	1.32	1.76
K00752.01	10797460	3.737	4.47	0.12	0.89	0.87	2.26
K00752.02	10797460	3.737	4.47	0.12	0.89	0.87	2.79
K00757.01	10910878	3.701	4.46	0.11	0.89	1.28	6.07
K00757.02	10910878	3.701	4.46	0.11	0.89	1.28	4.12
K00757.03	10910878	3.701	4.46	0.11	0.89	1.28	2.69
K00767.01	11414511	3.743	4.45	0.20	0.93	0.98	11.93
K00780.01	11918099	3.700	4.60	0.10	0.75	1.12	2.46
K00787.01	12366084	3.757	4.43	0.30	1.05	1.15	3.33
K00787.02	12366084	3.757	4.43	0.30	1.05	1.15	4.04
K00794.01	2713049	3.742	4.35	-0.04	1.07	1.15	2.44
K00801.01	3351888	3.744	4.32	0.30	1.24	1.21	10.87
K00806.01	3832474	3.723	4.34	0.11	0.98	1.04	9.91
K00806.02	3832474	3.723	4.34	0.11	0.98	1.04	13.78
K00806.03	3832474	3.723	4.34	0.11	0.98	1.04	2.20
K00829.01	5358241	3.762	4.40	0.03	1.09	1.22	3.54
K00829.02	5358241	3.762	4.40	0.03	1.09	1.22	2.35
K00829.03	5358241	3.762	4.40	0.03	1.09	1.22	3.88
K00834.01	5436502	3.753	4.17	0.18	1.31	1.43	7.64
K00834.02	5436502	3.753	4.17	0.18	1.31	1.43	2.84
K00834.03	5436502	3.753	4.17	0.18	1.31	1.43	2.30
K00834.04	5436502	3.753	4.17	0.18	1.31	1.43	1.47
K00844.01	6022556	3.758	4.46	-0.01	0.99	1.22	4.48
K00847.01	6191521	3.741	4.22	0.20	1.22	1.64	7.65
K00861.01	6685526	3.721	4.67	-0.12	0.72	0.99	1.76
K00873.01	7118364	3.760	4.34	0.13	1.15	1.65	2.62
K00874.01	7134976	3.697	4.47	0.17	0.84	1.05	2.39
K00874.02	7134976	3.697	4.47	0.17	0.84	1.05	1.60
K00881.01	7373451	3.700	4.46	0.06	0.85	1.18	3.89
K00881.02	7373451	3.700	4.46	0.06	0.85	1.18	5.18
K00896.01	7825899	3.726	4.55	0.15	0.84	0.96	4.33
K00896.02	7825899	3.726	4.55	0.15	0.84	0.96	3.08
K00897.01	7849854	3.767	4.39	0.14	1.10	1.07	13.28
K00906.01	8226994	3.701	4.50	0.00	0.80	1.02	2.42
K00906.02	8226994	3.701	4.50	0.00	0.80	1.02	2.66
K00906.03	8226994	3.701	4.50	0.00	0.80	1.02	1.04
K00918.01	8672910	3.719	4.46	0.17	0.91	1.07	11.03
K00934.01	9334289	3.745	4.36	-0.03	1.07	1.24	4.63
K00934.02	9334289	3.745	4.36	-0.03	1.07	1.24	2.94
K00934.03	9334289	3.745	4.36	-0.03	1.07	1.24	3.37

Table 3—Continued

Planet ID	Parent star (KIC ID)	$\log(T_{\text{eff}})$ (K)	$\log(g)$ (cgs)	[Fe/H]	$R_*$ ( $R_{\odot}$ )	$R_*^{\text{revised}}/R_*^{\text{KSAS}}$	$R_p$ ( $R_{\oplus}$ )
K00935.01	9347899	3.786	4.13	0.02	1.58	1.43	7.83
K00935.02	9347899	3.786	4.13	0.02	1.58	1.43	7.26
K00935.03	9347899	3.786	4.13	0.02	1.58	1.43	5.75
K00935.04	9347899	3.786	4.13	0.02	1.58	1.43	2.69
K00938.01	9415172	3.727	4.32	0.30	1.10	1.27	4.02
K00938.02	9415172	3.727	4.32	0.30	1.10	1.27	1.76
K00938.03	9415172	3.727	4.32	0.30	1.10	1.27	2.21
K00939.01	9466668	3.744	4.46	0.18	0.92	1.01	1.58
K00939.02	9466668	3.744	4.46	0.18	0.92	1.01	1.58
K00939.03	9466668	3.744	4.46	0.18	0.92	1.01	1.14
K00939.04	9466668	3.744	4.46	0.18	0.92	1.01	1.66
K00943.01	9513865	3.703	4.35	0.19	0.96	1.21	2.70
K00994.01	1431122	3.724	4.32	0.23	1.17	1.27	1.70
K00998.01	1432214	3.764	4.15	0.11	1.53	1.61	44.85
K01015.01	8158127	3.771	4.00	-0.02	1.70	1.56	4.13
K01015.02	8158127	3.771	4.00	-0.02	1.70	1.56	2.18
K01052.01	5956342	3.773	4.27	-0.01	1.19	1.25	3.04
K01052.02	5956342	3.773	4.27	-0.01	1.19	1.25	2.08
K01053.01	5956656	3.744	4.32	0.23	1.10	1.37	1.72
K01059.01	6060203	3.730	4.37	0.08	1.01	1.36	1.30
K01067.01	8246781	3.780	4.24	-0.11	1.18	1.15	42.24
K01069.01	8222813	3.705	4.42	0.19	0.87	0.79	3.16
K01069.02	8222813	3.705	4.42	0.19	0.87	0.79	1.77
K01089.01	3247268	3.759	4.34	0.11	1.11	1.08	10.12
K01089.02	3247268	3.759	4.34	0.11	1.11	1.08	5.51
K01099.01	2853093	3.762	4.29	0.20	1.18	1.43	8.04
K01102.01	3231341	3.771	4.05	-0.04	1.70	1.54	4.48
K01102.02	3231341	3.771	4.05	-0.04	1.70	1.54	4.23
K01106.01	3240158	3.781	4.36	0.00	1.11	1.19	2.64
K01161.01	10426656	3.727	4.36	-0.00	1.02	1.23	2.03
K01161.02	10426656	3.727	4.36	-0.00	1.02	1.23	2.46
K01161.03	10426656	3.727	4.36	-0.00	1.02	1.23	1.53
K01163.01	10468940	3.729	4.38	-0.06	1.05	1.38	2.09
K01163.02	10468940	3.729	4.38	-0.06	1.05	1.38	1.91
K01198.01	3447722	3.787	4.15	0.06	1.48	1.24	3.69
K01198.02	3447722	3.787	4.15	0.06	1.48	1.24	2.45
K01198.03	3447722	3.787	4.15	0.06	1.48	1.24	3.63
K01198.04	3447722	3.787	4.15	0.06	1.48	1.24	1.89
K01203.01	3962243	3.762	4.47	-0.22	0.95	1.00	2.91
K01203.02	3962243	3.762	4.47	-0.22	0.95	1.00	2.43
K01203.03	3962243	3.762	4.47	-0.22	0.95	1.00	2.78
K01219.01	3440861	3.694	4.46	0.10	0.83	1.05	0.67
K01226.01	6621116	3.725	4.21	0.30	1.22	1.49	52.77
K01239.01	6607286	3.751	4.24	-0.04	1.20	1.24	1.96
K01239.02	6607286	3.751	4.24	-0.04	1.20	1.24	2.16
K01240.01	6690082	3.743	4.34	0.14	1.06	1.28	1.74
K01240.02	6690082	3.743	4.34	0.14	1.06	1.28	2.99
K01261.01	8678594	3.747	4.04	-0.01	1.55	1.61	11.70
K01261.02	8678594	3.747	4.04	-0.01	1.55	1.61	3.37
K01268.01	8813698	3.764	4.23	-0.05	1.27	1.19	14.04
K01276.01	8804283	3.74	4.40	0.17	0.99	1.20	2.44
K01276.02	8804283	3.74	4.40	0.17	0.99	1.20	1.49
K01278.01	8609450	3.768	4.47	-0.09	1.01	1.19	2.20
K01278.02	8609450	3.768	4.47	-0.09	1.01	1.19	2.89

Table 3—Continued

Planet ID	Parent star (KIC ID)	$\log(T_{\text{eff}})$ (K)	$\log(g)$ (cgs)	[Fe/H]	$R_{\star}$ ( $R_{\odot}$ )	$R_{\star}^{\text{revised}}/R_{\star}^{\text{KSAS}}$	$R_p$ ( $R_{\oplus}$ )
K01301.01	10538176	3.724	4.49	-0.09	0.90	1.18	2.81
K01301.02	10538176	3.724	4.49	-0.09	0.90	1.18	2.59
K01305.01	10730034	3.708	4.37	0.03	0.94	1.25	1.57
K01305.02	10730034	3.708	4.37	0.03	0.94	1.25	1.40
K01306.01	10858691	3.764	4.45	-0.05	1.02	1.16	1.46
K01306.02	10858691	3.764	4.45	-0.05	1.02	1.16	1.62
K01306.03	10858691	3.764	4.45	-0.05	1.02	1.16	1.67
K01307.01	10973814	3.741	4.34	0.15	1.02	1.04	3.14
K01307.02	10973814	3.741	4.34	0.15	1.02	1.04	2.66
K01312.01	10963242	3.786	4.29	0.08	1.29	1.25	2.00
K01337.01	4243911	3.716	4.57	0.29	0.87	1.14	1.30
K01355.01	7211141	3.754	4.12	0.11	1.52	1.95	9.29
K01364.01	6962977	3.722	4.43	0.11	0.90	0.99	3.42
K01364.02	6962977	3.722	4.43	0.11	0.90	0.99	2.68
K01364.03	6962977	3.722	4.43	0.11	0.90	0.99	2.57
K01364.04	6962977	3.722	4.43	0.11	0.90	0.99	1.94
K01364.05	6962977	3.722	4.43	0.11	0.90	0.99	1.74
K01367.01	6934291	3.705	4.48	-0.00	0.85	1.22	1.72
K01407.01	9007866	3.722	4.35	0.06	1.03	1.25	0.95
K01425.01	11254382	3.751	4.28	0.12	1.21	1.41	3.15
K01429.01	11030711	3.752	4.46	0.30	1.01	1.17	5.62
K01432.01	11014932	3.742	4.35	0.07	1.01	1.17	2.52
K01432.02	11014932	3.742	4.35	0.07	1.01	1.17	2.04
K01432.03	11014932	3.742	4.35	0.07	1.01	1.17	1.55
K01439.01	11027624	3.772	4.06	0.11	1.64	0.99	7.74
K01472.01	7761545	3.747	4.48	0.14	0.93	1.28	6.85
K01503.01	12400538	3.75	4.23	0.13	1.21	1.77	5.94
K01527.01	7768451	3.729	4.28	0.08	1.14	0.93	4.03
K01567.01	5438099	3.695	4.47	-0.03	0.84	1.00	2.45
K01567.02	5438099	3.695	4.47	-0.03	0.84	1.00	1.93
K01567.03	5438099	3.695	4.47	-0.03	0.84	1.00	2.21
K01567.04	5438099	3.695	4.47	-0.03	0.84	1.00	2.69
K01574.01	10028792	3.751	4.09	0.11	1.59	1.89	11.15
K01582.01	4918309	3.731	4.17	-0.02	1.36	1.75	11.58
K01589.01	5301750	3.768	4.13	-0.05	1.43	1.45	3.23
K01589.02	5301750	3.768	4.13	-0.05	1.43	1.45	3.43
K01589.03	5301750	3.768	4.13	-0.05	1.43	1.45	3.50
K01589.04	5301750	3.768	4.13	-0.05	1.43	1.45	1.84
K01589.05	5301750	3.768	4.13	-0.05	1.43	1.45	2.85
K01590.01	5542466	3.691	4.47	-0.05	0.81	1.15	1.90
K01590.02	5542466	3.691	4.47	-0.05	0.81	1.15	1.37
K01601.01	5438757	3.743	4.34	-0.01	1.06	1.30	1.98
K01627.01	6543893	3.783	4.04	-0.24	1.64	2.15	4.59
K01627.02	6543893	3.783	4.04	-0.24	1.64	2.15	3.10
K01641.01	10879038	3.762	4.50	0.12	0.97	1.06	1.38
K01647.01	11153121	3.755	4.29	0.19	1.17	1.11	2.14
K01647.02	11153121	3.755	4.29	0.19	1.17	1.11	2.13
K01647.03	11153121	3.755	4.29	0.19	1.17	1.11	1.19
K01688.01	6310636	3.767	4.07	0.13	1.51	1.98	1.85
K01720.01	10015937	3.720	4.54	-0.18	0.75	1.17	2.56
K01739.01	7199906	3.748	4.10	0.08	1.51	1.82	3.37
K01750.01	6209677	3.736	4.48	0.17	0.89	1.00	1.29
K01820.01	8277797	3.733	4.45	0.10	0.90	0.55	2.06
K01820.02	8277797	3.733	4.45	0.10	0.90	0.55	1.26

Table 3—Continued

Planet ID	Parent star (KIC ID)	$\log(T_{\text{eff}})$ (K)	$\log(g)$ (cgs)	[Fe/H]	$R_*$ ( $R_{\odot}$ )	$R_*^{\text{revised}}/R_*^{\text{KSAS}}$	$R_p$ ( $R_{\oplus}$ )
K01849.01	9735426	3.722	4.49	0.11	0.89	1.22	2.96
K01858.01	8160953	3.732	4.33	-0.02	1.06	1.10	4.77
K01858.02	8160953	3.732	4.33	-0.02	1.06	1.10	2.19
K01860.01	4157325	3.753	4.27	0.11	1.14	1.07	2.61
K01860.02	4157325	3.753	4.27	0.11	1.14	1.07	2.52
K01860.03	4157325	3.753	4.27	0.11	1.14	1.07	1.63
K01866.01	9520838	3.737	4.32	0.09	1.09	1.18	4.59
K01882.01	6205228	3.757	4.27	0.14	1.26	1.58	2.38
K01891.01	8680979	3.688	4.47	0.15	0.81	1.17	2.15
K01891.02	8680979	3.688	4.47	0.15	0.81	1.17	1.46
K01922.01	9411166	3.759	4.33	0.11	1.20	1.37	2.43
K01922.02	9411166	3.759	4.33	0.11	1.20	1.37	1.81
K01931.01	10978763	3.728	4.32	0.01	1.10	1.46	2.09
K01931.02	10978763	3.728	4.32	0.01	1.10	1.46	1.81
K01931.03	10978763	3.728	4.32	0.01	1.10	1.46	1.64
K01952.01	7747425	3.750	4.33	0.03	1.17	1.18	2.15
K01952.02	7747425	3.750	4.33	0.03	1.17	1.18	2.38
K01952.03	7747425	3.750	4.33	0.03	1.17	1.18	1.44
K01974.01	7289577	3.729	4.36	0.07	1.00	1.38	3.65
K01992.01	11450414	3.747	4.12	-0.02	1.40	1.50	2.48
K02022.01	8564674	3.759	4.49	0.14	0.96	1.10	1.97
K02022.02	8564674	3.759	4.49	0.14	0.96	1.10	2.19
K02038.01	8950568	3.730	4.22	0.11	1.24	1.49	2.94
K02038.02	8950568	3.730	4.22	0.11	1.24	1.49	3.25
K02038.03	8950568	3.730	4.22	0.11	1.24	1.49	2.30
K02038.04	8950568	3.730	4.22	0.11	1.24	1.49	2.38
K02044.01	9656252	3.763	4.47	0.30	1.04	1.08	3.70
K02051.01	7265298	3.759	4.38	-0.01	1.11	1.07	3.03
K02051.02	7265298	3.759	4.38	-0.01	1.11	1.07	1.70
K02066.01	3239671	3.740	4.30	-0.04	1.17	1.40	4.30
K02083.01	7097965	3.769	4.21	0.24	1.35	1.20	2.32
K02087.01	6922710	3.771	4.22	0.08	1.37	1.11	1.71
K02095.01	7918992	3.764	4.40	0.06	1.11	1.57	1.45
K02103.01	7620413	3.747	4.39	0.08	0.98	1.10	1.32
K02107.01	9225395	3.728	4.47	-0.12	0.82	1.08	2.18
K02111.01	8612275	3.738	4.49	0.11	0.93	0.94	1.57
K02111.02	8612275	3.738	4.49	0.11	0.93	0.94	2.30
K02116.01	8164012	3.772	4.05	-0.00	1.69	1.94	2.42
K02121.01	9415108	3.729	4.33	0.08	1.01	1.34	1.74
K02147.01	10404582	3.760	4.43	0.06	1.01	1.49	2.45
K02160.01	5546761	3.763	4.26	-0.05	1.18	1.55	2.40
K02164.01	7204981	3.729	4.40	0.00	0.93	1.30	1.53
K02168.01	11308499	3.768	4.34	-0.03	1.18	1.24	1.60
K02168.02	11308499	3.768	4.34	-0.03	1.18	1.24	1.99
K02171.01	11410904	3.761	4.51	0.17	0.97	1.11	1.49
K02177.01	10965588	3.703	4.41	0.02	0.89	1.35	2.57
K02210.01	4142847	3.690	4.59	-0.08	0.71	1.13	1.43
K02215.01	7050060	3.783	4.27	0.03	1.36	1.47	1.22
K02218.01	12058204	3.747	4.33	0.14	1.05	1.31	1.77
K02218.02	12058204	3.747	4.33	0.14	1.05	1.31	1.72
K02220.01	6871071	3.751	4.09	0.12	1.59	1.80	2.16
K02220.02	6871071	3.751	4.09	0.12	1.59	1.80	2.43
K02220.03	6871071	3.751	4.09	0.12	1.59	1.80	2.05
K02224.01	8892157	3.757	4.49	0.08	0.94	1.09	1.49

Table 3—Continued

Planet ID	Parent star (KIC ID)	$\log(T_{\text{eff}})$ (K)	$\log(g)$ (cgs)	[Fe/H]	$R_{\star}$ ( $R_{\odot}$ )	$R_{\star}^{\text{revised}}/R_{\star}^{\text{KSAS}}$	$R_p$ ( $R_{\oplus}$ )
K02224.02	8892157	3.757	4.49	0.08	0.94	1.09	2.19
K02261.01	3734418	3.704	4.35	0.08	0.95	1.17	1.26
K02261.02	3734418	3.704	4.35	0.08	0.95	1.17	0.99
K02282.01	6751874	3.768	4.15	-0.06	1.46	1.68	2.19
K02286.01	8973129	3.738	4.43	-0.12	0.87	1.18	2.00
K02294.01	6934986	3.747	4.18	0.30	1.41	1.53	3.60
K02296.01	11498128	3.743	4.25	-0.00	1.21	1.25	2.61
K02307.01	7661065	3.724	4.52	0.07	0.83	1.04	1.95
K02310.01	11718144	3.739	4.52	0.07	0.88	1.07	2.05
K02317.01	10684670	3.745	4.38	0.30	1.07	0.93	1.19
K02319.01	9003401	3.782	4.28	0.07	1.30	1.06	1.81
K02373.01	10798331	3.746	4.27	0.18	1.18	1.20	2.64
K02374.01	9364290	3.749	4.27	0.11	1.17	1.35	1.59
K02374.02	9364290	3.749	4.27	0.11	1.17	1.35	2.63
K02383.01	9395024	3.752	4.28	0.08	1.25	1.30	1.77
K02392.01	7382313	3.746	4.44	-0.06	0.93	1.12	1.30
K02407.01	12120484	3.773	4.26	0.18	1.35	1.47	2.03
K02410.01	8676038	3.749	4.51	-0.11	0.90	0.99	2.49
K02410.02	8676038	3.749	4.51	-0.11	0.90	0.99	2.54
K02420.01	7107802	3.745	4.29	0.11	1.14	1.30	1.65
K02430.01	3533469	3.733	4.43	0.02	0.99	1.06	1.42
K02437.01	5036705	3.789	4.21	0.10	1.38	1.23	1.72
K02483.01	9851662	3.741	4.52	-0.07	0.90	1.14	1.31
K02509.01	9880190	3.699	4.39	0.02	0.92	1.22	1.24
K02521.01	7183745	3.699	4.49	-0.18	0.77	1.07	2.37
K02521.02	7183745	3.699	4.49	-0.18	0.77	1.07	1.51
K02543.01	12469800	3.694	4.48	-0.02	0.80	1.30	1.48
K02552.01	8757824	3.784	4.30	-0.01	1.21	1.22	1.41
K02571.01	6867588	3.717	4.55	0.19	0.82	1.11	1.12
K02601.01	7531677	3.768	4.20	0.00	1.32	1.09	1.01
K02624.01	8429314	3.763	4.33	0.01	1.12	1.29	3.70
K02628.01	10070468	3.765	4.19	-0.08	1.32	1.34	1.44
K02637.01	9574179	3.755	4.29	0.01	1.22	1.28	0.95
K02656.01	8636539	3.789	4.36	-0.01	1.20	1.22	1.34
K02658.01	8547429	3.763	4.38	0.22	1.11	1.16	1.34
K02730.01	8415200	3.747	4.20	0.03	1.25	1.37	1.30
K02869.01	7767162	3.802	4.22	0.15	1.36	1.07	1.33
K02920.01	7090524	3.741	4.26	0.24	1.32	1.46	1.55
K02931.01	8611257	3.698	4.49	-0.03	0.85	1.13	2.12